Evolution of genotypic and phenotypic diversity in multispecies biofilms

Cristina I. Amador[1], Sofia Zoe Moscovitz[1], Lorrie Maccario[1], Jakob Herschend[1 2], Isabel-Sophie Kramer[1], Hannah Jeckel[3], Vaughn S. Cooper[4], Knut Drescher[3], Thomas R. Neu[5], Mette Burmølle[1] and Henriette L. Røder[1 6 #]

[1]Section of Microbiology, Department of Biology, University of Copenhagen, Copenhagen, Denmark

[2]Present address: Functional Food, Novozymes A/S, 2800, Lyngby, Denmark

[3]Biozentrum, University of Basel, Switzerland

[4]University of Pittsburgh, Pittsburgh, USA

[5]Department of River Ecology, Helmholtz Centre for Environmental Research - UFZ, Magdeburg, Germany

[6]Pressent address: Section of Microbiology and Fermentation. Department of Food Science, University of Copenhagen. Rolighedsvej 26, 1958 Frederiksberg C, Denmark.

Author correspondence to h.lyng.roeder@food.ku.dk

Running title: Evolution in structured and non-structured multispecies community

Keywords: multispecies, bacterial interactions, biofilm, matrix, adaptive evolution, sporulation

Abstract

The fitness and adaptability of bacteria in microbial communities can be influenced by the interactions among the community partners, as well as specific spatial organisation. Here, we investigated the evolutionary dynamics of *Bacillus thuringiensis* in response to the presence or absence of spatial structure and bacterial interspecies interactions. During evolution experiments, a distinct phenotypic variant of *B. thuringiensis* frequently occurred, irrespective of the conditions tested: planktonic vs. biofilm or monospecies vs. mixed species. Remarkably, selection significantly favored this variant of *B. thuringiensis* over its ancestor in biofilm settings and when coexisting with *Pseudomonas defluvii* and *Pseudomonas brenneri*, co-isolated from a wastewater facility. Interestingly, the evolved phenotype displayed lower biomass in mixed species biofilms, shorter generation time, and lacked sporulation compared to the ancestor. The strains displaying this phenotypic variation contained mutations in the regulator *spo0A* that initiates sporulation but also de-represses expression of matrix determinants in other Bacilli. Consistently, matrix proteomics revealed a reduced abundance of TasA in the phenotypic variant, a major biofilm matrix component in *Bacillus* species, while higher abundance was found in co-culture with *P. brenneri*. Our results indicate that interspecies interactions within biofilms not only promote *B. thuringiensis* diversification but also select for altered traits such as reduced biofilm matrix production. Moreover, *P. brenneri* was favoured in co-culture biofilm vs. planktonic settings, suggesting that spatial structure and *B. thuringiensis* diversification facilitate species co-existence. These findings could impact applications where *Bacillus* and *Pseudomonas* are utilized in consortia, such as plant growth promoters or biopesticides.

Introduction

When encountering new environmental challenges, bacterial populations can adapt their physiological state (phenotype) through different mechanisms: expressing specific traits, acquiring new advantageous mutations (*de novo* genetic variation), or utilizing the pre-existing genetic diversity within the population (standing genetic variation) [1–3]. Besides intraspecific variation, natural communities contain many species that might either constrain adaptation by competing for resources, e.g., via niche exclusion [4], or facilitate adaptation by making new niches available [5, 6]. In biofilms, microbial cells are in close proximity and can influence each other´s phenotypes and evolutionary trajectories through social interactions [7]. Spatial segregation in biofilms increases the frequency of interactions between cells of the same genotype and favors cooperative behaviors but can also support variants that are otherwise outcompeted in unsegregated environments [8–10] and facilitate coexisting populations [11, 12]. Several studies have reported that competitive interactions within biofilms are dominant, including competition for limited space and resources [10, 13–16]. However, evidence shows that competition can subside locally over time, often leading to stable coexistence [17]. We have previously described that interspecies interactions can lead to evolved variants that display enhanced mutualism in biofilms [18–20]. Thus, to better understand bacterial adaptation mechanisms in natural environments, investigations of adaptation mechanisms in the presence of spatial structure and multiple species that co-occur in natural communities are crucial.

The evolution of social interactions within biofilms has been extensively studied in various Gram-negative bacteria, including *Pseudomonas spp*. and *Burkholderia cenocepacia* [21–23]. However, comparatively less attention has been devoted to investigate evolutionary processes of Gram-positive bacteria, especially in the presence of multiple species. Although some studies have explored the adaptive evolution of Gram-positive bacteria in diverse biofilm systems, their focus has primarily been on adaptive genotypes [24–26] or co-culture [20, 27].

In this study, we aim to specifically examine the influences of cultivation conditions and interspecies interactions on the diversification of *Bacillus thuringiensis* (BT), a Gram-positive, spore-forming bacterium renowned for its insecticidal capabilities [28]. BT was cultured in isolation and in combination with *Pseudomonas defluvii* (PD) and *Pseudomonas brenneri* (PB), both of which were co-isolated with BT from a wastewater treatment facility in Kalundborg,

Denmark [29]. *Bacillus* spp. and *Pseudomonas* spp. are known for their utility as plant growth enhancers and biopesticides [30]. Importantly, research has demonstrated that such bacterial consortia manifest unique, emergent properties not attainable by individual species alone [31]. Additionally, the rationale behind selecting these species for our investigation stemmed from their potential synergistic contributions to biofilm formation, a premise supported by preliminary laboratory findings. In contrast to prior studies that primarily focused on the dynamics of biofilm dispersal and recolonization over short evolutionary spans, here our aim was to study cells that consistently remained adherent [20, 32]. This led to the identification of a phenotypic variant of BT, termed the "light variant," from its reduced Congo red dye binding in colonies on agar, compared to the ancestral strain. This light variant, which arose frequently and we found to be linked to mutations in sporulation genes, demonstrated a remarkable capability to dominate and replace the ancestral strain in most conditions examined. Crucially, the dominance of this evolved phenotype was amplified in mixed-species cultures and within biofilm contexts, underlining the effects of both biotic and abiotic complexity on evolutionary dynamics. This finding sheds light on the adaptive strategies of BT within microbial consortia.

Results

Regular emergence of a BT phenotypic variant after short-term evolution assay

We investigated how the presence of other species influenced the selection of new phenotypic variants of BT in biofilm or planktonic conditions. For the biofilm condition, cells were required incubated in TSB with a submerged polycarbonate slide. This initial phase was followed by removing the polycarbonate slides, washing the slides with PBS to remove unattached cells, and transferring the slides (with the attached cells) to new wells containing fresh media, followed by incubation for another 24 h. This process was repeated for eight consecutive cycles. At the conclusion of the experiment, we plated and enumerated the cultures based on distinct colony morphology (Figure 1a).

A particular BT phenotypic variant was detected in all replicate evolution experiments, which we termed "light variant" as it bound less Congo red compared to the ancestor (Figure 1b and S1). The population size of the ancestral BT did not differ among treatments despite the culture composition (mono-culture, two-species culture, or multispecies-culture, Figure 1b). However, the BT light variant independently emerged in each evolved biofilm population where it consistently grew to significantly higher CFU counts than the ancestral BT strain. On the contrary, analogous evolution experiments in liquid culture showed no significant difference in CFU counts between the ancestral BT and BT light variant within each culture condition (Figure 1b). Still, the variant phenotype was found to be significantly more prevalent than its ancestor regardless of the cultivation settings — biofilm or planktonic — when not considering the species combination (Wilcoxon´s test, $p_{\text{Biofilm}} = 2.84\text{x}10^{-16}$; $p_{\text{Plank}} = 0.0013$, Figure 1b). Data from these short-term evolution experiments suggest that the BT light variant exhibited higher fitness under biofilm conditions and in the presence of PB and/or PD when compared to the ancestral BT strain.

During the evolution experiment, all species were maintained. However, the trajectories of *Pseudomonas* species varied depending on the culture condition and design, as shown in Figure 1c. BT outcompeted both *Pseudomonas* species in planktonic settings (Figure 1c, right panel). These findings indicate that the lack of spatial structure and resulting intermixing may limit the co-existence of different species. However, in biofilm conditions (as shown in Figure 1c, left panel), PB abundance increased in mixed-species conditions while PD decreased. This suggests that the adapted BT phenotype may facilitate co-existence of BT and PB in biofilm settings.

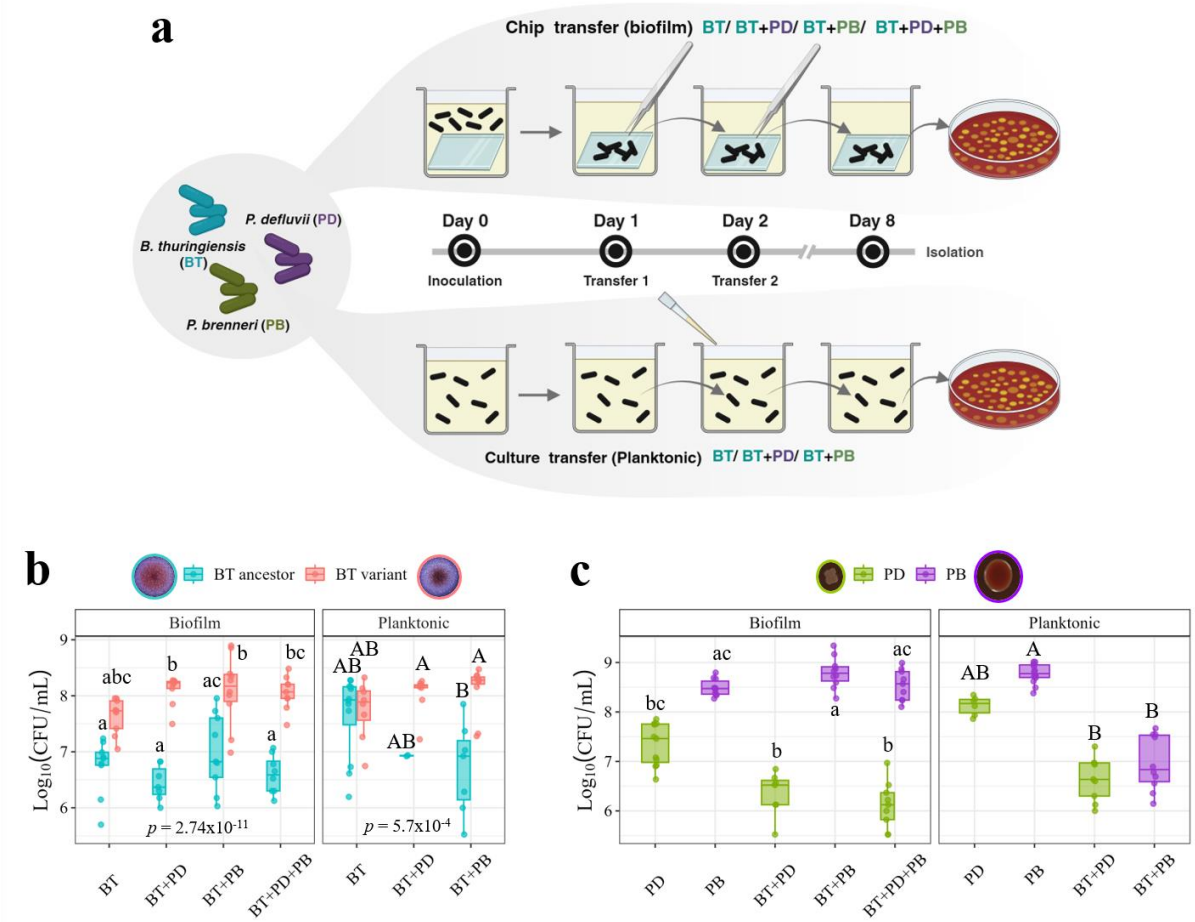

Figure 1. Short-term evolution assay of *Bacillus thuringiensis* (BT) in the presence/absence of *Pseudomonas* species. (a) Experimental setup: BT was cultured alone or with *Pseudomonas brenneri* (PB) and/or *Pseudomonas defluvii* (PD) in Tryptic Soy Broth (TSB) medium, either as planktonic or biofilm cultures, for 24 hours. Biofilm samples were transferred daily onto fresh medium for eight days, followed by plating and CFU counting. **(b)** BT cell counts (Log_{10}(CFU/mL)) of variant (red) and ancestor (blue) phenotypes in different strain combinations, presented for biofilm (left) and planktonic (right) cultures. Box plots represent ≥ 3 biological replicates, represented as individual points, each averaged from 3 technical replicates. Different letters denote significance per facet (Dunn´s post-hoc test, $p < 0.05$). Significance of a Wilcoxon´s test comparing BT ancestor and variant regardless of combination is indicated by p (< 0.05). **(c)** Cell counts (Log_{10}(CFU/mL)) of PD (green) and PB (purple) in various strain combinations and culture conditions. Box plots represent ≥ 7 biological replicates, represented as in (b). Different letters denote significance per facet (Dunn´s post-hoc test, $p < 0.05$).

The BT "light variant" exhibited distinct phenotypic traits compared to its ancestor

We isolated 150 BT light variants from independent experiments and conditions, all sharing the same phenotypic traits. While the ancestral BT and the BT light variant displayed different colony morphology, they also had visibly different phenotypes during growth in liquid

cultures: In non-shaking conditions, the ancestral BT cells sank to the bottom of the culture, whereas the BT light variant remained in suspension (Figure S1, right panel). This phenotype, known as auto-aggregation, occurs in many bacterial species. It involves bacteria attaching to each other rather than to a surface, forming macroscopic clumps that settle at the bottom of culture tubes. [48, 49]. Moreover, some environmental *Bacillus licheniformis* have been documented to undergo aggregation during suspension culture under carbon limitation or glucose-free conditions [50, 51] Thus, we hypothesize that the observed sedimentation by the BT ancestor could be related to auto-aggregation, unlike the variants.

Besides these phenotypic traits, the BT light variant was unable to produce spores unlike the ancestral BT strain, as evidenced by optical microscopy (not shown). Out of the 150 isolated light variants, all of them had identical visible phenotypic traits. Therefore, we focused on four light variants, namely V1, V2, V3, and V6, and further investigated their characteristics. These light variants were selected from different culture conditions and independent experiments: V1 and V2 were isolated from biofilm co-cultures with PB in separate experiments, whereas V3 and V6 were isolated from BT biofilm mono-cultures (Table S1).

We measured the capacity for spore formation of both ancestral and variant strains in planktonic settings over four days. These assays demonstrated that, irrespective of the incubation period, the variants did not produce spores, whereas the ancestral BT strain consistently produced spores regardless of the incubation time (Figure 2a). Next, we investigated whether other species may influence spore formation in the ancestor. The ability to form spores was assessed in mono-, two-species-, or multispecies biofilm conditions for 24-hour biofilms; however, no significant difference was observed between the tested combinations (Figure 2b).

We hypothesized that selection for growth rate may have favored the loss of spore production by BT light variants since sporulation is an energy-intensive process. Growth curves were performed for the BT ancestor and the BT light variants in TSB. We found that the four BT light variants consistently showed a significantly faster doubling time (t_{gen}) and growth rate (r) compared to their ancestor (Table S2). Consequently, the time required to reach half of the maximum culture yield was significantly lower (t_{mid} or ½ k). This data suggests that the BT light variants have a growth advantage compared to the ancestral BT when competing for resources with the *Pseudomonas* species. This may also have led to the higher CFU counts observed in

mixed-species cultures during our short-term evolution experiments in biofilms and planktonic cultures.

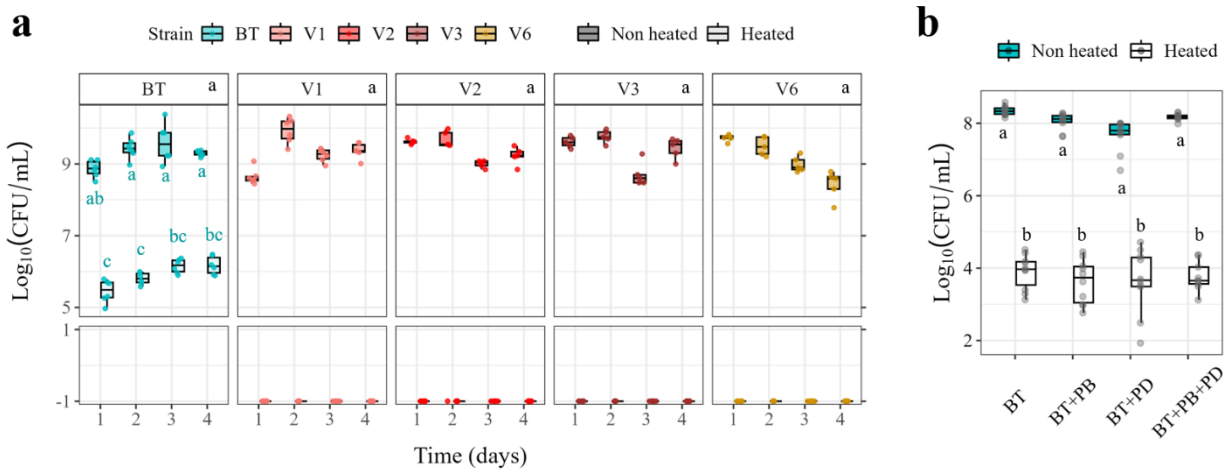

Figure 2. Ability of spore formation for *B. thuringiensis* ancestor or variant phenotypes. Box plots represent Log_{10}(CFU/mL) of *B. thurgingiensis* ancestor (BT) and variants under control (vegetative cells, non-heated) and boiling (germinating spores, heated) conditions. Box plots show Log_{10}(CFU/mL) in non-heated or heated conditions where individual points indicate biological replicates. Different letters denote significant differences ($p < 0.05$, Dunn´s post-hoc test, Bonferroni correction). **(a)** Spore formation in planktonic monocultures over 1-4 days incubation. Log_{10}(CFU/mL) values were adjusted by adding 0.1 to accommodate zero values (represented as -1). $n \geq 5$ biological replicates. Black letters denote significant differences between strains only considering non-heated conditions, while turquoise letters indicate comparisons within BT (heated vs. non-heated). **(b)** Spore formation ability of BT ancestor in biofilm settings in different strain combinations after one-day incubation; $n \geq 10$ biological replicates.

BT light variants displayed mutations in sporulation-related genes

Whole genome sequencing of BT light variants and the BT ancestor revealed that the light variants displayed mutations in sporulation-related genes. This correlated with the observed lack of sporulation in all the phenotypes. Variants V1, V3, and V6 contained mutations that resulted in the *spo0A* gene's loss of function, but of different types (as depicted in Figure 3a). The *spo0A* gene encodes a response regulator that, in its phosphorylated active form, activates the transcription of early sporulation genes and, consequently, the initiation of sporulation (Figure 3b) [52, 53]. For variants V1 and V3, large deletions were observed in this region. Specifically, V1 lacked a 1.5 kb fragment containing most of *spo0A* and CDS0080 genes, whereas V3 had a 4.5 kb deletion that also included the *spoIVB* and *recN* genes (as shown in Figure 3a). V6 only contained a non-synonymous mutation in the *spo0A* gene (C151>T), resulting in a change in the amino acid sequence Q51>stop, leading to early termination and, thus, loss of function of Spo0A. These

mutations were confirmed by Sanger sequencing using specific primers (data not shown). The mutations found in *spo0A* undoubtedly explain the non-sporulating phenotype for variants V1, V3, and V6, given the central role of *spo0A* and *spoIVB* in the sporulation process. However, for V2, it was not possible to confirm any clear link to the expected mutations or junction links to the observed phenotype.

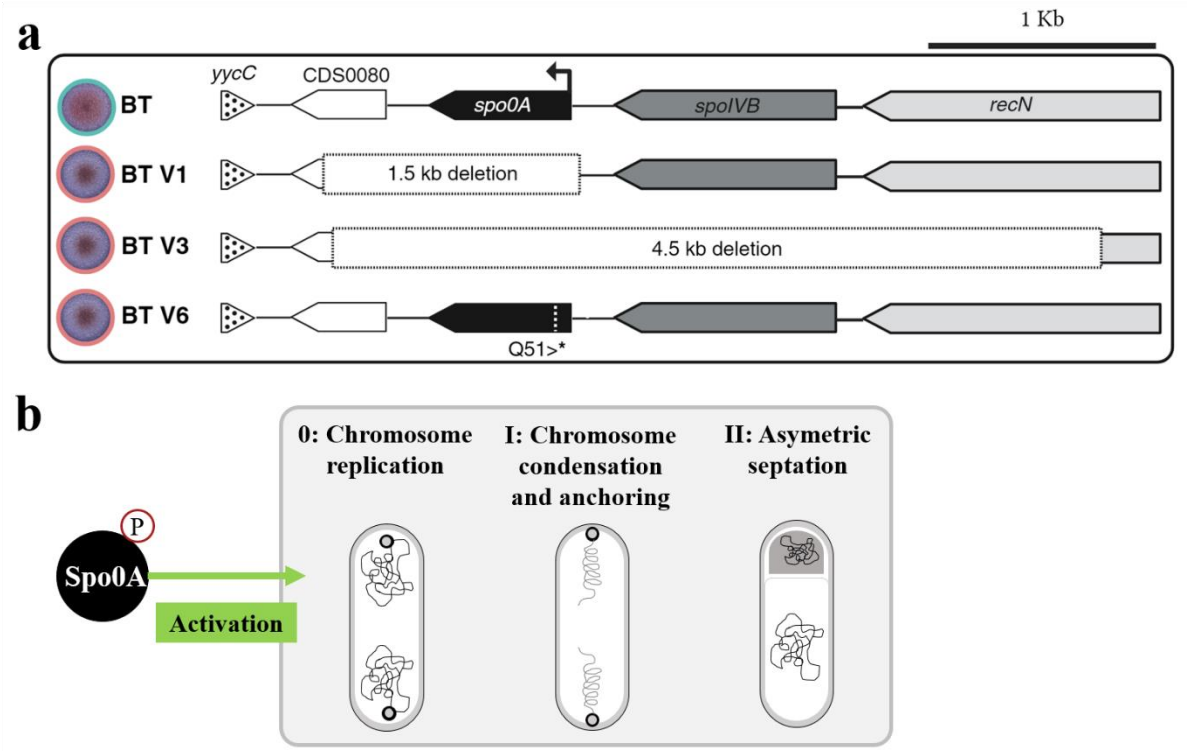

Figure 3. Mutations in *B. thuringiensis* variants compared to the ancestor and its effect on sporulation pathway. (a) Mutations found in the selected variants (BT Vx, circled pink) compared to their ancestor (BT, circled blue). Dashed boxes indicate large deletions in variants V1 and V3. Q51>* in variant V6 indicates a change in amino acid 51 of the *spo0A* gene from Q to stop codon (*). **(b)** Role of SpoA for activation of the sporulation pathway in *Bacillus* sp. Phosphorylated Spo0A activates transcription of genes involved in sporulation stages 0, I, and II [86, 87].

Reduced biofilm matrix production in mixed biofilms with the adapted variant

The BT light variant phenotype showed increased CFU counts compared to the ancestor after the eight-day evolution experiment, especially in biofilm settings. We thus wondered whether population size in biofilm settings may correlate with improved biofilm formation of the evolved phenotype. We measured the total amount of biofilm formed (including cells and matrix) on the slides after 24 hours by quantification of crystal violet retention as an overall estimate of biofilm biomass. We also quantified specific prevalence of each strain by CFU counts of both the BT

ancestor and V1 variant (as shown in Figure 4). Biofilm biomass was similar for the BT ancestor and variant in mono-culture. Co-cultivation with PB or in multispecies induced biofilm biomass for both ancestor and variant, however, only significantly for the ancestral phenotype (Figure 4a). These results suggest differential adhesion or matrix production in mixed cultures. Mono- and co-culture biofilms of variants V2, V3, and V6 reproduced the observed results for the ancestor and V1 variant, indicating that the origin of the variants did not influence their biofilm phenotype (Figure S2a).

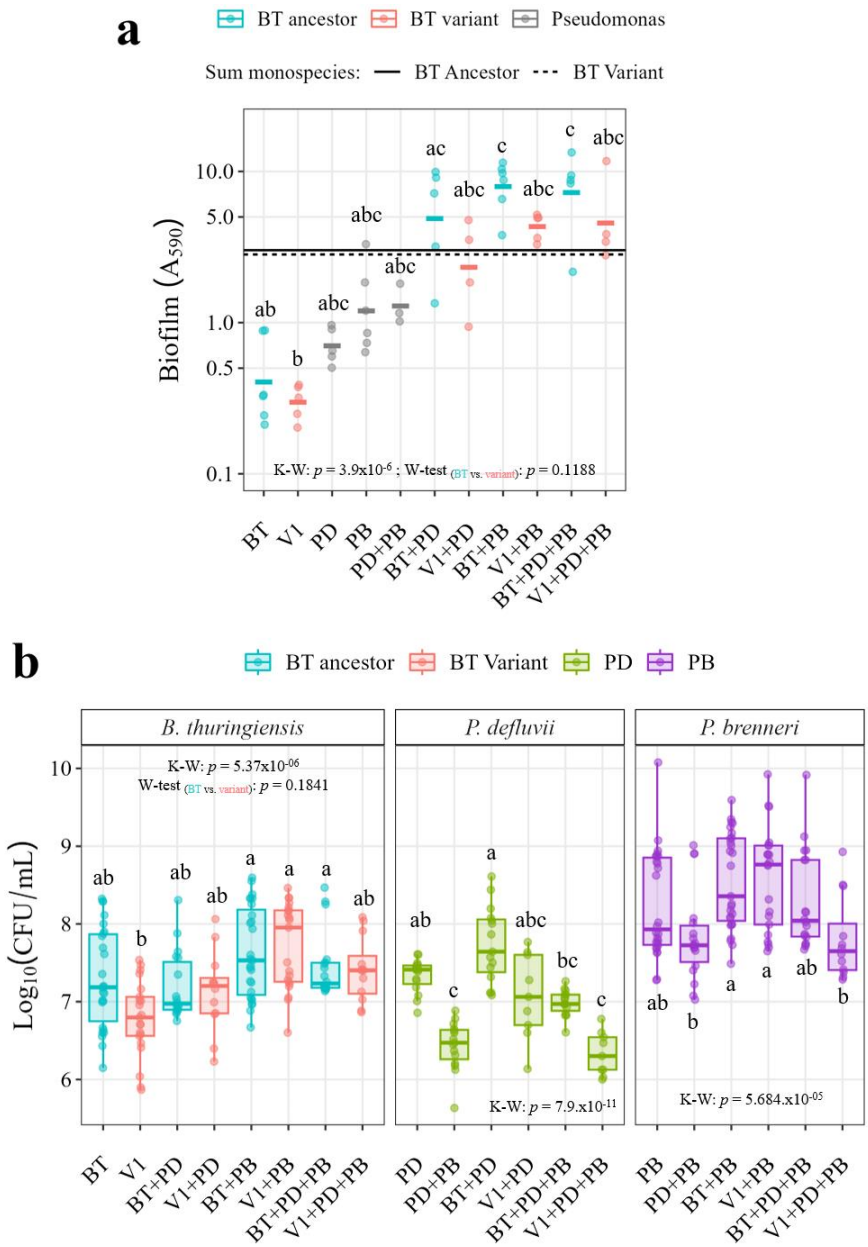

Figure 4. Biofilm formation of *B. thuringiensis* ancestor, V1 variant and *Pseudomonas* in mono- or mixed-species cultures after 24 h. BT: *B. thuringiensis* ancestor (blue); V1: *B. thuringiensis* V1 variant

(red); PD: *P.defluvii*; PB: *P.brenneri*. Adhesion was measured in mono-culture biofilms or in co-culture with *P. defluvii*, *P. brenneri* or both (multispecies) in TSB medium after 24 h. K-W: significance of a Kruskal-Wallis test, testing all combinations within each panel ($p < 0.05$). Dissimilar letters are indicative of significant differences per panel, with $p < 0.05$ (Dunn´s post-hoc test). W-test$_{(BT\ vs.\ variant)}$: indicates significance of a Wilcoxon´s rank sum test, comparing biomass (A_{590}) or CFUs based on BT phenotype. **(a)** Mean biofilm measured as CV stained biomass (A_{590}). Data based on ≥ 4 biological replicates, represented as individual points. Each biological replicate consisted of 6 technical replicates. Horizontal lines represent the theoretical multispecies biofilm biomass based on the sum of mono-culture biomass. **(b)** Biofilm counts per mL of *B. thuringiensis, P. defluvii and P. brenneri*. Data based on ≥ 9 biological replicates, represented as biological replicates, each consisting of ≥ 3 technical replicates. Dissimilar letters show significance per species.

The CV results suggested differential adhesion or matrix production in mixed cultures with the variant phenotype. Thus, we next quantified CFU counts for each species in the different combinations to measure specific adhesion. Cell counts of the BT ancestor and V1 variant within culture condition were not significantly different (Figure 4b, left panel), indicating similar surface colonization for both strains. However, the variant cell counts were significantly induced in co-culture with PB compared to V1 monoculture biofilms. Given that PB counts were unchanged despite the BT phenotype, we hypothesize that the adapted phenotype benefitted from co-cultivation with PB. CFU counts of the other variants replicated the observations found for V1 in mono- and co-culture with PB (Figure S2b). Remarkably, biofilm co-culture of the ancestor and V1 variant resulted in a 1.2 Log_{10} fold reduction in ancestor counts in just 24 h, confirming a higher fitness of the light variant (Figure S3, $p = 5.7 \times 10^{-4}$).

In contrast, neither *Pseudomonas* species grew to a higher density in co-culture compared to mono-culture conditions. Rather, PD experienced a reduction in cell counts when co-cultured with PB or in multispecies biofilms with the variant phenotype, indicating an antagonistic effect of the adapted phenotype and PB on PD (Figure 4b).

In conclusion, *we* observed reduced biofilm biomass (CV) in mixed-species biofilms with the light variant, but not adhesion (CFU counts). We propose that such differences may be due to reduced matrix production, either by the BT light variant, or by *Pseudomonas* spp.

Matrix glycan composition altered by co-cultivation and BT light variant

We observed a synergistic effect on biofilm biomass in mixed species, compared to mono-culture, though only significantly different with BT ancestor (Figure 4a). However, no correlation was found between such induction and CFU counts of either of the strains. We hypothesized that

such differences in biofilm biomass between ancestor and variant in mixed species might imply altered production of biofilm matrix, either in BT variants or the *Pseudomonas* species. Thus, we investigated the influence of interspecies interactions and/or acquired mutations on the amount and types of glycans within the biofilm matrix.

We screened multispecies biofilms (BT+PD+PB), including 78 different fluorescent lectins binding to carbohydrates of varying nature (Table S3). After filtering the binding results by fluorescence signal (data not shown), three lectins with strong binding in multispecies biofilms were identified for further analysis: AAL, WGA, and RCA. AAL binds α-fucose-containing polymers, WGA binds N-acetylglucosamine (GlcNAc), and RCA binds galactose and N-acetylgalactosamine (Gal/GalNAc) glycans [39]. Considering the minimal difference in biofilm biomass between co-culture and multispecies biofilms (Figure 4a), we used co-culture conditions as it closely resembled multispecies conditions. Therefore, we assessed binding of the three lectins to BT mono- and co-culture biofilms with PB, for both ancestral and variant strains.

AAL lectin bound to BT cells and certain matrix-like structures in BT mono-culture biofilms, while the variants displayed a reduced lectin signal (Figure 5a). This indicates that the composition of glycoconjugates in the cell wall or surface differed between the variants, leading to differential AAL binding. Image quantification of lectin binding supported visual observations, significantly reducing lectin binding in the variants (Figure 5b). However, the amount of lectin binding per biofilm volume (biovolume) unit was not significantly changed in the variants (Figure 5c). We cannot exclude the possibility that intrinsic heterogeneity of biofilm and differences among slide replicates, even within biological replicate, could account for these results. Moreover, some of the replicates also showed some unspecific lectin binding that could influence the analysis.

Co-cultivation of BT ancestor or variants with PB however showed similar AAL binding, (Figure S4), suggesting a change in glycoconjugates triggered by interspecies interactions. Moreover, PB also showed AAL binding in mono-culture and, thus, association of lectin signal with the specific matrix producer may be cumbersome in co-culture conditions (Figure S4, BT and PB panels).

Unlike AAL lectin binding, no differential binding was observed for RCA lectin, regardless of the BT genotype or cultivation (mono- vs. co-culture with PB). Moreover, in PB biofilms, this lectin bound thin filaments that revealed a galactose/N-Acetylgalactosamine polymer network

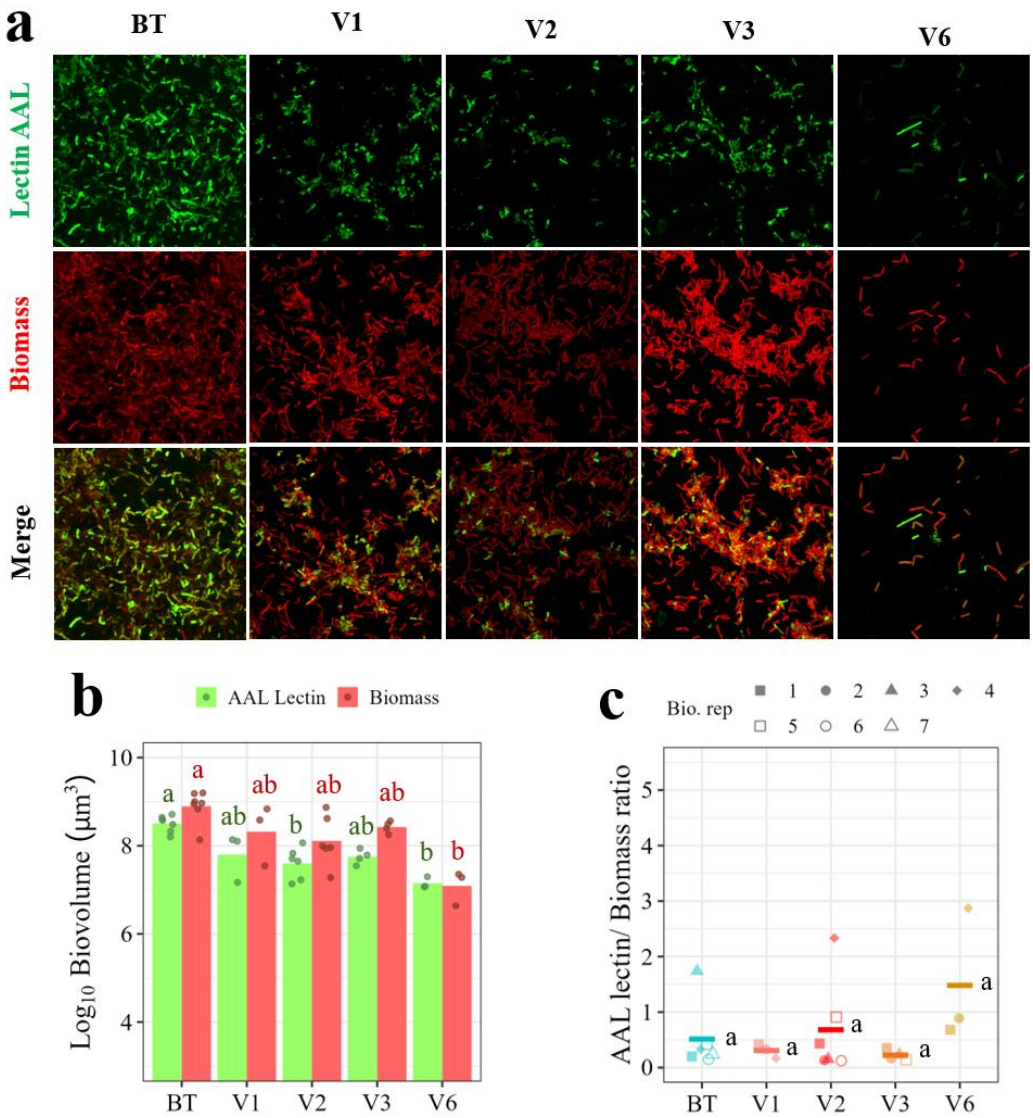

Figure 5. AAL lectin staining in mono-culture biofilms of *B. thuringiensis* ancestor and variant strains. BT: *B. thuringiensis* ancestor; V1: variant1, V2: variant 2; V3: variant 3; V4: variant 4; PB: *P. brenneri*. Biomass: red fluorescent signal of biofilms stained with the cell biomass stain Syto60. Lectin AAL: green fluorescent signal of biofilms stained with the fluorescent lectin AAL-FITC. Merge: combined fluorescent signal of cell biomass and lectin stains. **(a)** Maximum intensity projection (MIP) images of Z-stacks recorded by confocal laser scanning microscopy for 24-hour biofilms. The scale of the images is 124 µm across. **(b)** Biofilm volume (Biovolume, μm^3) of lectin (green) and cell biomass fluorescence (red). Biovolume was calculated using BiofilmQ [40] per channel, based on ≥ three biological replicates (represented as points) and two images per replicate. Bars show mean values per channel. Dissimilar letters denote significant p-value (Dunn´s post-hoc test, $p < 0.05$) per channel (green = lectin; red = cell biomass). **(c)** Ratios of lectin biovolume/ biomass biovolume for each strain. Data based on ≥ three biological replicates, represented by different symbols, and two images per replicate. Crossbars indicate the mean ratio for each strain. Dissimilar letters denote significant p-value (Dunn´s post-hoc test, $p < 0.05$).

(Figure S5a). On the other hand, WGA bound to BT cell surfaces (Figure S5b), likely the cell wall because this lectin binds to the sugar GlcNAc, which is a major component of peptidoglycan [54]. However, there was no visible difference observed in either the variants or mixed-species combinations (data not shown).

In conclusion, even though AAL lectin staining showed a tendency of reduced production of α-fucose polymers by BT variants, lectin-biomass ratios were not conclusive. However, other matrix components may be influenced by the distinct phenotypic biofilm formation by BT genotype, such as protein abundance.

Matrix protein abundance of BT light variant decreased in response to co-cultivation and genotype

We next investigated the effects of interspecies interactions and acquired mutations in BT on the proteomes of biofilm matrices, hoping to explain the reduced biofilm matrix production observed in either the BT variants or the *Pseudomonas* species. We specifically examined variants V1 and V6 due to their distinct origin of isolation (V1 from co-culture with PB and V6 from mono-culture), in order to eliminate the possibility that the isolation origin influenced the abundance of matrix proteins. Our proteomic experiments utilized a chemical extraction of biofilm matrix as input material, which results in a lower number of expected proteins compared to total biofilm samples.

First, we performed a comparative analysis of BT proteomes by phenotype (variants *vs*. ancestor) and culture condition (mono-culture vs. co-culture with PB) (Figure 6). The analysis showed that BT ancestor mono-culture samples were the most distinct from the rest, clustering together on the right of PC1 (Figure 6a), as evidenced by probabilistic principal component analysis (PPCA). The variation in PC1 was driven by the BT phenotype (ancestor vs. variant), while the cultivation condition (mono-culture vs. co-culture) determined PC2. Light variant co-culture or mono-culture samples could not be discriminated, while BT ancestor co-culture samples were grouped in a distinct cluster compared to mono-culture. Interestingly, BT co-culture proteomes overlapped with variant mono- and co-culture proteomes. Consistently, comparison of BT ancestor vs. variants in mono-culture evidenced the largest difference in proteomes. Only 20 proteins out of 187 were common to all three BT strains (Table S5 and Figure 6c) and 11 significantly changed, related to amino acid and carbohydrate metabolism energy production, among others. In contrast, 150

proteins were exclusively detected in the ancestor (Table S6), indicating a major reduction in protein abundance in both variants. Among those, different proteins

involved in sporulation or regulated by the Stage 0 sporulation protein, Spo0A, were only detected in the ancestor, consistent with sporulation-defective phenotypes observed in the variants. To discard unique expressions due to detection limits, we calculated the mean and 0.05 percentile of each proteome to use as a cutoff (Table S4 and Figure 5b). However, DivIVA, SpoVG, immune inhibitor A (CDS_04360 and CDS_05099), neutral protease B (CDS_00401) and the major biofilm matrix component (CDS_ 04363 and CDS_04365) were still above the expression cutoff in the BT ancestor, compared to the light variants. Remarkably, the four latter proteins were also more abundant in the ancestral co-culture (Table S8), suggesting that their abundance is influenced by BT phenotype —ancestor — and the presence of PB.

Co-cultivation of PB with BT ancestor or variant phenotypes reduced biofilm matrix protein abundance by 90 % (17 proteins co-culture vs. 187 in mono-culture), suggesting that PB minimized the differences of BT proteomes (Figure 6d). However, 15 proteins were uniquely detected in the ancestor co-culture, including the four mentioned above (Table S7). Mono-culture vs. co-culture comparisons rendered highly different results depending on the phenotype compared. In the ancestor pairwise analysis, 111 out of 163 proteins were only detected in mono-culture (Figure 6e, Table S8), supporting the previous observation that PB decreased abundance of biofilm matrix-associated proteins in BT. However, comparisons between the V1 and V6 variants resulted in reduced matrix proteomes, with 15 and 5 proteins detected, respectively (Tables S9, S10 and Figures 6f-g).

We hypothesize that the acquired mutations may switch off the expression of multiple genes involved in sporulation, a highly complex and tiered-regulated process linked to biofilm formation. There is previous evidence that *spo0A* mutations in *Bacillus subtilis* enhanced maintenance metabolism [55] and increased glucose consumption and acetate formation [56]. This would be consistent with the faster doubling time observed for the variants, given that fewer proteins and consequently a lower amount of energy, are required in the absence of sporulation.

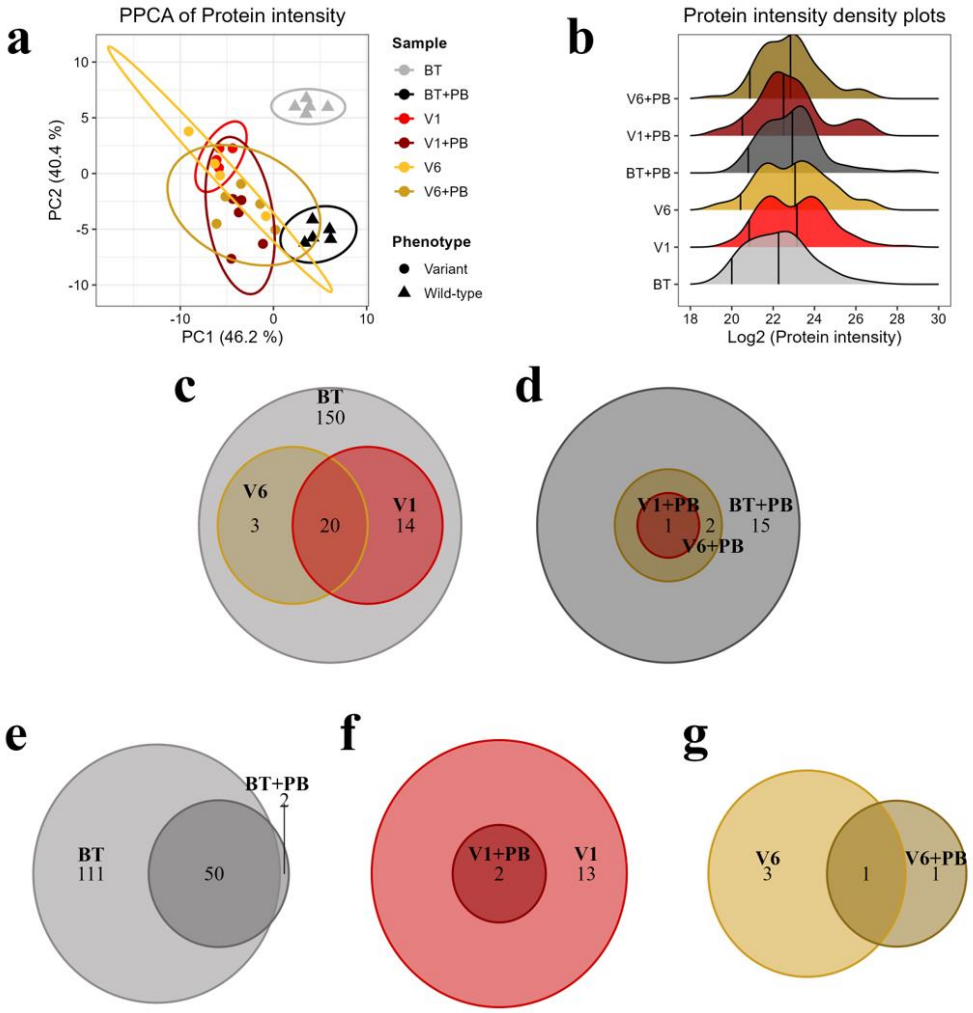

Figure 6. Differential protein abundance in *B. thuringiensis* ancestor *or variants* in mono-culture vs. co-culture biofilms with *P. brenneri*. BT = *B. thuringiensis*; PB = *P. brenneri*; V1 = *B. thuringiensis* variant 1; V6 = *B. thuringiensis* variant 6. **(a)** Probabilistic PCA plot of all monoculture and co-culture proteomes, based on Log_2 transformed protein intensity data with 5 biological replicates per sample. Color indicates the sample type and shape the phenotype: wild-type (triangles) or variant (circles). Ellipses indicate sample group clustering based on the principal components. **(b)** Density plots of Log_2 transformed protein intensity for mono-culture vs. co-culture samples representing 5 biological replicates. Percentile 0.05 is indicated as the leftmost vertical line, while middle lines denote protein intensity means for each sample excluding NA values (no protein detected). **(c-g)** Venn diagrams of *B. thuringiensis* mono-culture proteomes (c), co-culture proteomes (d), or mono-culture vs. co-culture proteomes (e-f), considering proteins detected in ≥ 60 % of each sample (3/5 biological replicates). **(c)** Mono-culture proteomes, total proteins detected = 187. BT, n = 187 proteins; V1, n = 34 proteins; V6, n = 23 proteins. **(d)** Co-culture proteomes, total proteins detected = 18. BT+PB, n = 18 proteins; V1+PB, n = 1 protein; V6+PB, n = 3 proteins. **(e)** BT vs. BT+PB proteomes, total proteins = 163. BT, n = 161 proteins; BT+PB, n = 52. **(f)** V1 vs. V1+PB proteomes, total proteins = 15. V1, n = 15 proteins; V1+PB, n = 2. **(g)** V6 vs. V6+PB proteomes, total proteins = 5. V6, n = 4 proteins; V6+PB, n = 2.

We investigated whether matrix proteins were differentially abundant in PB based on culture condition and BT phenotype (Figure S6). Out of 169 detected proteins, mono- and co-culture proteomes showed similar mean abundance and 0.05 quantiles (Table S4 and Figure S6a). Unlike BT results, co-cultivation did not strongly affect the number of detected proteins, with 64% shared among all samples (n = 108) (Figure S6b). PB mono-culture samples clustered separately to co-culture samples, indicating that cultivation drove PC1 (Figure S6c). Seventeen proteins were uniquely detected in co-culture with BT ancestor (Table S11), though co-culture samples with BT, V1, or V6 could not be discriminated in the PPCA. While no unique or differentially abundant matrix proteins were found in PB, multiple proteins involved in amino acid transport and metabolism varied based on culture condition. Co-cultivation reduced the abundance of several amino acid transporters in PB (arginine, branched-chain, cysteine, glutamate/aspartate, and putrescine), regardless of BT phenotype (Figure S6d). Other proteins involved in branched-changed transport (braC_1), glycine, tyrosine or arginine/ornithine metabolism were only detected in PB monoculture (Table S11).. These findings suggest that PB optimizes amino acid utilization differently depending on environmental conditions. In co-culture with BT, ecological dynamics might shift, altering metabolic priorities and protein abundance. This aligns with our previous observation that the V1 variant increased CFU counts in co-culture with PB, suggesting it benefits more from co-cultivation with PB than its ancestor (Figure 4b).

Based on all proteomics results, we hypothesize that the lower abundance of matrix-associated proteins in BT light variants correlates with the previously observed reduction in biofilm biomass in the variant mixtures. Furthermore, the absence of differential or unique abundance of matrix proteins in PB suggests a deficiency in BT's production of matrix components associated with *spo0A* mutations. These results are also consistent with the observed tendency of reduced AAL lectin binding.

Discussion

Microbial interactions influence the fitness, survival, and evolution of interacting species, enabling better resource utilization, mitigating competition, enhancing mutual dependencies, or optimizing nutrient exchange. Despite their predominance and significance, adaptive evolution experiments focusing on multispecies biofilms remain limited. This study aimed to address this gap by examining effects of interspecies dynamics and spatial structuring on trait selection within the Gram-positive bacterium BT.

Here, we used short-term evolution assays where BT, PD, and PB were cultured individually or in combination, under both planktonic and biofilm conditions (Fig. 1a). Throughout, these assays, a distinct phenotypic variant of BT, which we termed "light variant", consistently emerged. Notably, this variant was more prevalent than its ancestral counterpart in biofilm environments (Fig. 1b), with its selection further amplified by interactions with *Pseudomonas* species, indicating a potentially fitter phenotype under such conditions. While previous experimental evolution studies in biofilms have documented the emergence of adapted variants exhibiting enhanced biofilm characteristics relative to their ancestors, our findings diverge [18, 20, 57, 58]. For instance, Lin and collaborators identified a "fuzzy spreader" phenotype of *B. thuringiensis* in a bead-transfer evolution study, where all adapted lineages resulted in enhanced biofilm production compared to its ancestor [26]. In contrast, the BT variants identified in our study produced less biofilm within mixed-species contexts, which was associated with a reduction in biofilm matrix components like TasA. Despite this, the adapted phenotype prevailed across different environments (planktonic or biofilm, Fig. 1b), suggesting a fitness advantage over the ancestral form. This advantage is consistent with the observed shorter generation time of the non-sporulating variants and higher prevalence of the light variant V1 when co-cultured with the ancestor (Figure S3). However, considering the comparable biofilm characteristics between the ancestor and the variants, our findings suggest that BT adaptation in biofilms may be driven by factors beyond adhesion or biofilm formation, such as nutrient competition and subsequent metabolic optimization, which may also be more compatible with *Pseudomonas* co-existence.

Biofilm formation and spore production are two different survival strategies of bacteria facing adverse environmental stresses. However, intertwined regulatory pathways between biofilm formation and sporulation have been proposed for both *B. subtilis* and *Bacillus cereus* [59, 60]. *spo0A* mutants in other *Bacilli* such as *Bacillus velezensis*, *B. subtilis* or *B. cereus* are impaired in

biofilm formation, since Spo0A de-represses EPS production and promotes biofilm [61–64]. Whole-genome sequencing of the variants linked lack of sporulation with mutations in key genes regulating sporulation (Fig. 5). V1, V3 and V6 variants harbored mutations in *spo0A*, which has a central role in sporulation [52, 53]. However, in this study, all selected variants of BT –lacking Spo0A– showed comparable CFU counts and matrix production to the ancestor in mono-culture. These findings suggest that, in the examined conditions, control of biofilm formation in BT may deviate from that previously reported for *B. subtilis* and *B. cereus*.

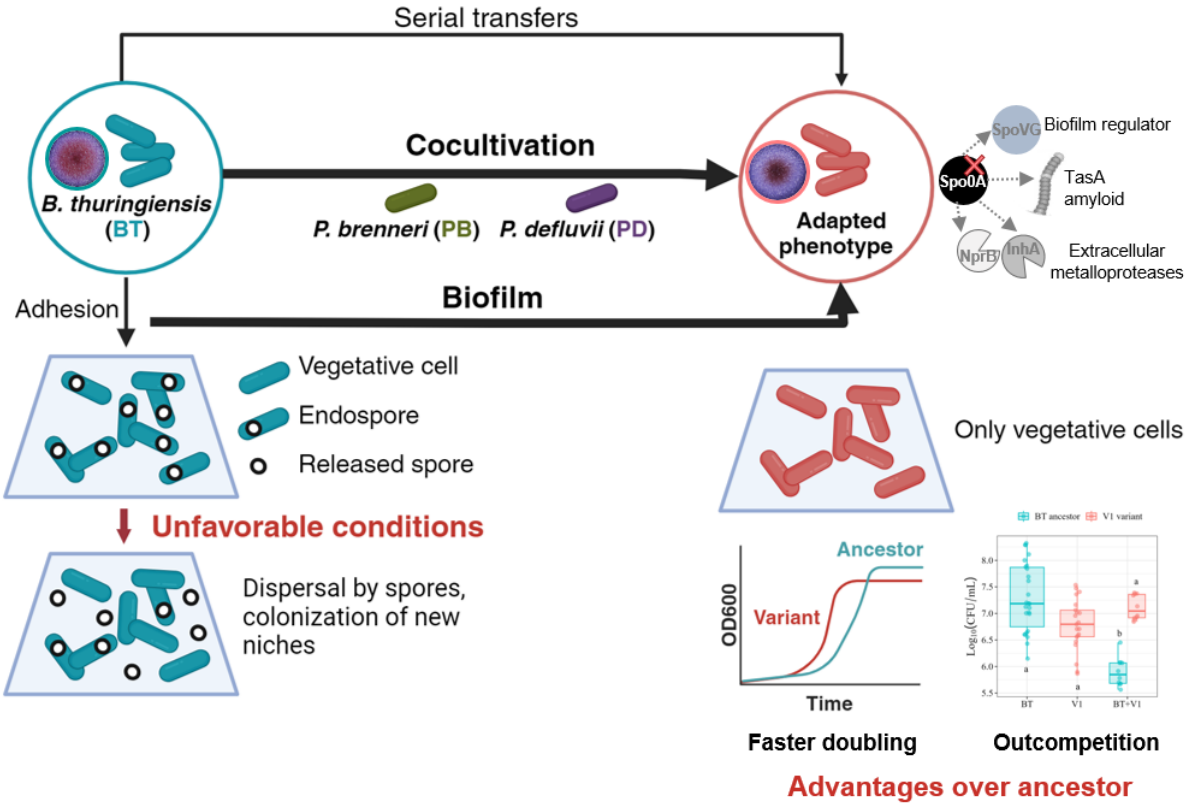

Figure 7. Proposed model for adaptation of the evolved variants. *B. thuringiensis* non-sporulating variants emerged in all conditions, but biofilm settings and co-cultivation with either or both *P. brenneri* and *P. defluvii* enhanced selection of the variant (thicker arrows). In adverse conditions, spores might aid in dispersing biofilms in the ancestral strain. However, adapted variants, lacking sporulation, could experience restricted dispersal. The adapted variant lacks sporulation, displays faster doubling time than its ancestor and can outcompete it in co-culture biofilms. Variants lack proteins SpoVG, the matrix amyloid TasA and two extracellular metalloproteases involved in matrix recycling. Indirect Spo0A regulation is indicated by dashed arrows [52, 62, 73, 74, 79, 88].

A recent study established a link between spore formation and biofilm dispersal in *B. subtilis* [65]. Under unfavorable conditions, spores may detach from the biofilm, dispersing

through air, water, or other means, and potentially establishing new biofilms elsewhere, thereby promoting bacterial survival and spread. Our findings indicate that, under the controlled conditions of the laboratory where environmental stressors are minimal or absent, sporulation might become dispensable for BT (Figure 7). However, non-sporulating variants have also been reported in other Bacilli in more relevant ecological contexts, such as deep nutrient or energy deprivation, food surfaces or insect cadavers, where they survived from days to months [66–68]. This suggests that our findings can have ecological relevance and that such mutations can be selected and fit in more extreme conditions.

Irrespective of the particular mutations, all BT light variants grew faster than the ancestor (Table S2), did not sporulate (Figure 2b), and bound the AAL lectin less, which pointed towards decreased matrix glycoconjugates (Figure 4). Moreover, proteomic analysis revealed that different matrix proteins were uniquely detected the ancestor. Among these, two TasA/CalY orthologues and SpoVG were detected in BT ancestor but not in the variants (Table S6). TasA is a major matrix component in *Bacillus* biofilms and its absence results in significant defects in biofilm and pellicle formation in *B. subtilis* [69, 70]. Its paralog in *B. cereus* is needed for root colonization, while in *B. thuringiensis*, the TasA-orthologue CalY has been identified as a cell-surface adhesin and described as a major virulence factor and biofilm matrix protein [71, 72]. Interestingly, both CalY orthologues (*tasA_3* and *tasA_4*) are located in the same operon than *sipW*, regulated by SinR and, thus, indirectly by Spo0A in *B. cereus* (Figure S7), explaining our results. On the other hand, SpoVG plays a critical role in the spore-coat formation of *Bacillus anthracis* and is a regulator of both sporulation and biofilm formation in *B. cereus* 0-9 that activates the levels of Spo0A and, thus, the fate of *B. cereus* cells: biofilm or sporulation [73–75]. Proteomic results also evidenced the unique detection of two metalloproteases only in BT ancestor: NprB and InhA (immune inhibitor A), linked with protein recycling during sporulation and indirectly regulated by Spo0A [52, 76, 77]. InhA coding gene, *ina_4*, is also located in the same genomic region than the two *calY* orthologues and regulated by the SinI-R regulon in other Bacilli [78, 79]. We speculate that the lack of expression of TasA and the biofilm regulatory protein SpoVG could contribute to the differences observed between CFU counts and total biofilm biomass for the variant phenotype (CV).

Apart from BT genotype, co-cultivation was another factor influencing protein abundance, yet differently depending on the target species. Co-cultivation significantly altered the proteome

of BT but only in the ancestor (Figure 6a). Meanwhile, for PB the presence of BT greatly impacted protein abundance regardless of the phenotype (Figure S6c). An example was a consistent lower abundance of amino acid transporters in PB co-culture. (Figures S6d). This could indicate competition for resources or utilization or distinct metabolic pathways in co-culture. We have previously reported that cooperative interactions between community members can facilitate metabolic cross-feeding on specific amino acids, though in a different multispecies biofilm model [44, 80]. Additionally, previous studies have shown that coexistence can remain stable over time, for instance, by oppositely altering the pH or secreting costless by-products to the other species' benefit [33, 34, 81–84]. Most reported *Bacillus-Pseudomonas* co-cultures demonstrate either competition or amensalism, driven by bioactive natural products, while positive interactions are usually associated with cross-feeding or shared resources [31]. Our evolution experiment revealed significant reduction of PB CFU counts in planktonic co-culture with BT, unlike biofilm conditions, suggesting that spatial structure facilitates co-existence of these species. Furthermore, higher abundance of the variant phenotype was observed in co-culture with PB in both planktonic and biofilm settings, suggesting that the adapted phenotype benefits from PB, compared to its ancestor. Thus, we characterize this as a non-exploitable interaction between the BT variant phenotype and PB, that is, improved growth but not at the cost of the other species.

In summary, we found a higher selection pressure for non-sporulating variants of *B. thuringiensis* in a biofilm setting and in the presence of *Pseudomonas* species (Figure 7). Thus, our findings evidence the importance of considering population diversity, intra- and interspecific, as well as spatial structure as determinants of bacterial adaptation. Moreover, *Bacillus spo0A* mutants have proven survivability in relevant ecological contexts where stress factors are present, but also resulted beneficial in fermentation processes for enhanced enzyme or metabolite production [31, 85]. Therefore, the results of this study are relevant in biotechnological applications where consortia of such variants with *Pseudomonas* species could be employed to optimize and efficiently produce valuable products.

Methods

Strains and materials

The three bacterial strains PD, PB, BT were isolated from water samples collected at a wastewater treatment plant in Kalundborg, Denmark, and their genome s were sequenced in another study [29]. All strains were grown at 24 °C in Tryptic Soy Broth (TSB; 17 g pancreatic digest of casein, 3 g papaic digest of soybean meal, 5 g sodium chloride, 2.5 g dextrose, 2.5 g dibasic potassium phosphate in 1 l distilled water, pH 7.3), supplemented with 1.5 % agar when needed. To distinguish the bacterial strains and/or species variants, 40 µg/ml of Congo Red (Merck) and 20 µg/ml Coomassie Brilliant Blue G (Sigma-Aldrich) were added to the TSB base, referred to as TSB Congo Red plates. In previous studies, this media has facilitated identification of adapted variants and differentiation among species [33, 34].

Short-term evolution assay with spatial structure

Overnight cultures in TSB medium were adjusted to an optical density at 600 nm (OD_{600}) of 0.15 in fresh TSB prior to usage. The experiment was conducted in 24-well plates, where each well contained a polycarbonate chip (12 x 12 x 0.78 mm^3) (PC) that was diagonally tilted so that bacteria could adhere to both sides of the chip. In each well, 2 ml of OD_{600} 0.15 cultures were added, either as mono-species culture or mixed-species culture. For mixed-species conditions, 1:1 or 1:1:1 OD_{600} ratios of the species were used. Every 24 hours (h), the floating pellicle was gently removed before the polycarbonate chip was transferred to a new well, and the chip was washed thrice in 1x phosphate-buffered saline (PBS) to remove any leftover planktonic/pellicle cells. This was done consecutively for 8 days, followed by washing the PC chips before transferring to a 5-ml Eppendorf tube containing 2 ml 1x PBS. The biofilm was then removed from the PC surface by shaking at 600 rpm for 5 minutes (min) (Titramax1000, Heidolph). The resulting suspension was then plated on TSB Congo Red plates with three technical replicates to estimate colony forming units (CFUs) and to screen for new variants with different colony morphology.

Short-term evolution assay without spatial structure

To test selection pressure in conditions not favoring spatial structure, a short-term evolution assay was also performed with well-mixed planktonic cultures. Cultures were adjusted to OD_{600} = 0.15 as described above, and 5 ml of this culture was incubated overnight, with shakingat 250 rpm (KS 250 basic, IKA). After 24 h, 5 µl of this culture was transferred to new fresh media. The

transfer was repeated for 8 days, followed by plating on TSB Congo Red plates with three technical replicates.

Quantification of biofilm formation

Assessment of the biofilm formation on the polycarbonate surfaces was performed using a modified crystal violet assay [35]. Biofilms were allowed to grow on PC chips for 24 h as described above, washed thrice in 1x PBS and then transferred to a well of a 24-well plate containing 2 ml of 1 % crystal violet aqueous solution and incubated for 20 min in the dark. Then, the chips were carefully removed and rinsed five times in 1x PBS. Crystal violet stained chips were then incubated in 2 ml of 96 % ethanol for 30 min. The biofilm biomass was then quantified as the absorbance of crystal violet solution at 590 nm (A_{590}). To avoid measurement saturation, samples were diluted in 96% ethanol when A_{590} was higher than 1.

Growth curves in liquid cultures

Cultures of the wild-type and variants were grown overnight in liquid TSB medium. Then, 1:100 dilutions of the overnight cultures in TSB were prepared, and these cultures were used to inoculate 96-well plates, using 3 biological and 3 technical replicates. Growth was monitored for 24 h at 24 °C with 282 rpm double orbital shaking and OD_{600} readings every 10 min. Growth data was integrated to calculate different growth parameters using the Growthcurver R package [36] to determine different parameters. These included: t_mid, the point of inflection of the growth curve; K, carrying capacity or maximum size of the population; t_gen, generation time of a strain; r, intrinsic growth rate of a population; sigma, the fit goodness of the model.

Optical microscopy

Liquid cultures of the different strains were incubated for 24 h in TSB at 24 °C while shaking at 250 rpm. From these 24-h cultures, 10 µl were pipetted onto a microscope glass slide, and a coverslip was applied on top. Samples were observed with an Olympus BH2 optical microscope with 10x and 40x magnification objectives, with 0.25 and 0.65 numerical apertures, respectively.

Sporulation assay

To compare the sporulation capacity of *B. thuringiensis* and its variants, a sporulation assay was performed similarly to the description by Toukabri et al. [37]. Firstly, overnight cultures (24 h) of the ancestor and variants were serially diluted and plated on TSB Congo Red to quantify the concentration vegetative cells in each culture. Similarly, an aliquot of such cultures was heat-shocked at 80 ˚C for 20 min before plating on TSB Congo Red plates to quantify sporulating cells. Plates were incubated two days at 24 ˚C before counting. This was repeated for 3 consecutive days (48-, 72- and 96-h cultures) to assess whether incubation time influenced spore formation. Furthermore, the sporulation assay was performed for the biofilms grown on PC chips to estimate the number of spores produced in mono or mixed-species cultures.

Biofilm matrix staining with fluorescent lectins

Matrix glycoconjugate characterization in the three species community was performed using 78 different fluorescently labeled lectins (using FITC, AlexaFluor488, or Fluorescein) in combination with confocal laser scanning microscopy (TCS SP5X, Leica Germany, controlled by the software program LAS-AF vers. 2.41) as described previously by Neu and Kuhlicke [38, 39]. The lectins and fluorescent conjugates used are listed in Supplementary Table S3. Briefly, biofilms were grown on polycarbonate chips for 24 h, followed by washing three times with 1x PBS, as described above. Staining solutions containing fluorescent lectins were prepared at a concentration of 100 µg/ml (in filter-sterilized ultrapure water). 100 µl was then added to a biofilm on a polycarbonate chip, followed by incubation for 30 min in the dark. The excess staining solution was washed twice with dH_2O before adding SYTO60 to the sample, prior to confocal imaging. Excitation of FITC, AlexaFluor488, and Fluorescein was performed at 488 nm, and the emission signals were recorded from 500–580 nm. Excitation of SYTO60 was at 652 nm, and emission was recorded from 665-750 nm. For lectins conjugated to Rhodamine, excitation was done at 525 nm, and emission was recorded from 570-650 nm. Image data sets were recorded using 63x NA 0.9 and 63x NA 1.2 objective lenses with a step size of 0.5 µm.

Based on the screening, three lectins, *Aleuria aurantia* Lectin (AAL), Wheat Germ Agglutinin (WGA), and *Ricinus communis* Agglutinin (RCA), were chosen for further testing. Here, a dual species combination of *Pseudomonas brenneri* (PB) and *Bacillus thuringiensis* (BT) was used to better estimate the effects between, and on *Bacillus thuringiensis* and its variant when

co-cultured with *Pseudomonas*. Images of AAL-lectin-stained biofilms of BT and variants V1, V2, V3 and V6 were analyzed using the biofilm image analysis software suite BiofilmQ [40]. Biofilm volume (biovolume) was calculated for each fluorescent channel: lectin (FITC channel) and biomass (SYTO60 channel) with a minimum of 6 images per sample (3 biological replicates and 2 images per replicate). Moreover, biovolume ratios (AAL-lectin-stained biovolume divided by the total biovolume) were calculated per image.

Biofilm matrix proteome measurements

Biofilms were grown for 24 h in TSB medium on PC chips as described above, followed by washing 3 times in 1x PBS to remove planktonic cells and biofilm pellicle. Five biological replicates per condition were processed, each composed of five PC chips that were combined to extract sufficient amount of biofilm matrix material for proteomics analysis (technical replicates). The biofilm was then resuspended in 5 ml of 1x PBS by shaking at 1000 rpm for 10 min. The biofilm matrix was extracted using the formaldehyde and NaOH extraction method [41, 42]. Briefly, 0.006 V formaldehyde 37 % (30 µl) was added to the biofilm samples and incubated for 1 h at 4 °C while mixing, followed by addition of 0.4 V NaOH 1 N (2 ml) and incubation for 3 h at 4 °C while mixing. Samples were then dialyzed using 3500 MWCO 22 mm SnakeSkin™ Dialysis Tubing (ThermoFisher Scientific) against 2.5 l milliQ water, overnight at 4 °C with stirring. Protein content in dialyzed samples was quantified using the Bio-Rad Protein assay, a modified Bradford assay [43], before freezing with liquid nitrogen. Finally, the extracted biofilm matrix was lyophilized using an ALPHA 1-4 LDplus freeze dryer (Christ, VWR) and kept at -80 °C until sample preparation for proteomics.

For the proteomics sample preparation, digestion, mass spectrometry, and data analysis were conducted as described in Herschend et al. [44], with some modifications described in the supplementary methods. Reference genomes of *B. thuringiensis,* and *P. brenneri* were prepared as part of a previous study and are available online (NCBI) with IDs JARTVI000000000 and CP122540.1, respectively. The raw data and results of the mass spectrometry proteomics analysis by MaxQuant have been deposited to the ProteomeXchange Consortium via the PRIDE [45] partner repository with the dataset identifier PXD046156.

Whole-genome sequencing and analysis of variants

Genomes of BT ancestor and variants V1, V2, V3, and V6 (Table S1) were sequenced by extracting the DNA using DNeasy Blood & Tissue Kit (Qiagen) from overnight cultures. The samples were sequenced with short reads using Truseq libraries on the Illumina NovaSeq 6000 and 2x150 cycles (Novogene, UK).

Data was analyzed using breseq (v0.35.0) to call variants using the –p polymorphism flag when analyzing population sequences [46]. As the reference genome, we used the previously constructed hybrid assembly of long and short reads from BT, available online (NCBI) with ID JARTVI000000000. Mutations detected between our ancestral strain and the reference genome were not considered. The breseq software also predicts new junctions within the genome which may occur due to mobile element insertions, large deletions, structural rearrangements and prophage excision. These analyses were also included.

Statistical analysis and visualization

All analyses and plotting were done in RStudio v4.1.1 [47] and package "ggplot2" v3.4.2. All datasets were tested for normality and equal variance using the Shapiro-Wilk (base R) and Levene's (package "car" v3.1.2) tests, respectively. Most datasets were not normally distributed and thereby a Kruskal-Wallis test (base R) was used when comparing more than two groups, unless otherwise specified. A general expression was kruskal.test(log10_CFUmL~Combination), however the quantitative variable and categorical variables changed depending on the dataset. A Dunn´s post-hoc test was performed using package "FSA" v0.9.4 to consider multiple comparisons when the Kruskal-Wallis test was significant, with a Bonferroni correction. When comparing only two groups, a Wilcoxon´s rank test t-test was applied, usually comparing ancestor and variant phenotype (i.e. wilcox.test (CFU~Phenotype)). A *p*-value of 0.05 was used as a threshold for statistical significance ($p < 0.05$). Compact letter display for multiple comparisons was calculated using the R package "rcompanion" v2.4.35.

Author contributions

CIA is first author. Conceptualization and planning: HLR. Execution of experiments: HLR., SZM, ISK. Data analysis: CIA, HLR and LM. Manuscript preparation: CIA, HLR and MB, in consultation with JH, HJ, VSC, KD, TRN.

Competing interests

The authors declare no competing interests.

Acknowledgments

The authors thank Sara Olsen and Anette Løth for technical assistance, the DTU Proteomics core facility for technical assistance in proteomics sample preparation. Support by Ute Kuhlicke with lectin analysis and confocal laser scanning microscopy is highly appreciated. We thank the Villum Foundation for grants to MB (no. 10098) and HR (no. 34434) and the US Office of Naval Research, for grant N629091812174 to MB, as well as the Swiss National Science Foundation Consolidator Grant TMCG-3_213801 to KD, and the German Bundesministerium für Bildung und Forschung grant TARGET-Biofilms 16GW0245 to KD, funding this work.

Data availability statement

B. thuringiensis and *P. brenneri* genomes are available online at NCBI (https://www.ncbi.nlm.nih.gov/genome/) with the following IDs: JARTVI000000000 and CP122540.1, respectively. The mass spectrometry proteomics raw data and results from analysis by MaxQuant have been deposited to the ProteomeXchange Consortium via the PRIDE [45] partner repository with the dataset identifier PXD046156 (https://www.ebi.ac.uk/pride/archive). The data is currently private and can only be accessed with a single reviewer account that has been created. The data will be publicly available when accepted for publication. For reviewer access, use the username reviewer_pxd046156@ebi.ac.uk and password kkAMO14X.

References

1. Agrawal AA. Phenotypic plasticity in the interactions and evolution of species. *Science* 2001; **294**: 321–326.
2. Barrett RDH, Schluter D. Adaptation from standing genetic variation. *Trends Ecol Evol* 2008; **23**: 38–44.
3. Barrick JE, Lenski RE. Genome dynamics during experimental evolution. *Nat Rev Genet 2013 1412* 2013; **14**: 827–839.
4. Scheuerl T, Hopkins M, Nowell RW, Rivett DW, Barraclough TG, Bell T. Bacterial adaptation is constrained in complex communities. *Nat Commun 2020 111* 2020; **11**: 1–8.
5. Calcagno V, Jarne P, Loreau M, Mouquet N, David P. Diversity spurs diversification in ecological communities. *Nat Commun* 2017; **8**.
6. Emerson BC, Kolm N. Species diversity can drive speciation. *Nature* 2005; **434**: 1015–1017.
7. Nadell CD, Xavier JB, Foster KR. The sociobiology of biofilms. *FEMS Microbiol Rev* 2009; **33**: 206–224.
8. Gross K, Cardinale BJ. Does species richness drive community production or vice versa? Reconciling historical and contemporary paradigms in competitive communities. *Am Nat* 2007; **170**: 207–220.
9. Cardinale BJ, Wright JP, Cadotte MW, Carroll IT, Hector A, Srivastava DS, et al. Impacts of plant diversity on biomass production increase through time because of species complementarity. *Proc Natl Acad Sci U S A* 2007; **104**: 18123–18128.
10. Nadell CD, Drescher K, Foster KR. Spatial structure, cooperation and competition in biofilms. *Nat Rev Microbiol 2016 149* 2016; **14**: 589–600.
11. Rainey PB, Travisano M. Adaptive radiation in a heterogeneous environment. *Nat 1998 3946688* 1998; **394**: 69–72.
12. Habets MGJL, Rozen DE, Hoekstra RF, De Visser JAGM. The effect of population structure on the adaptive radiation of microbial populations evolving in spatially structured environments. *Ecol Lett* 2006; **9**: 1041–1048.
13. Foster KR, Bell T. Competition, not cooperation, dominates interactions among culturable microbial species. *Curr Biol* 2012; **22**: 1845–1850.
14. Xavier JB, Foster KR. Cooperation and conflict in microbial biofilms. *Proc Natl Acad Sci*

U S A 2007; **104**: 876–881.

15. Rao D, Webb JS, Kjelleberg S. Competitive interactions in mixed-species biofilms containing the marine bacterium Pseudoalteromonas tunicata. *Appl Environ Microbiol* 2005; **71**: 1729–1736.
16. Hibbing ME, Fuqua C, Parsek MR, Peterson SB. Bacterial competition: surviving and thriving in the microbial jungle. *Nat Rev Microbiol* 2010; **8**: 15.
17. Ghoul M, Mitri S. The Ecology and Evolution of Microbial Competition. *Trends Microbiol* 2016; **24**: 833–845.
18. Røder HL, Herschend J, Russel J, Andersen MF, Madsen JS, Sørensen SJ, et al. Enhanced bacterial mutualism through an evolved biofilm phenotype. *ISME J* 2018.
19. Liu W, Jacquiod S, Brejnrod A, Russel J, Burmølle M, Sørensen SJ. Deciphering links between bacterial interactions and spatial organization in multispecies biofilms. *ISME J* 2019; **13**: 3054–3066.
20. Henriksen NNSE, Hansen MF, Kiesewalter HT, Russel J, Nesme J, Foster KR, et al. Biofilm cultivation facilitates coexistence and adaptive evolution in an industrial bacterial community. *NPJ biofilms microbiomes* 2022; **8**.
21. McDonald MJ, Gehrig SM, Meintjes PL, Zhang XX, Rainey PB. Adaptive Divergence in Experimental Populations of Pseudomonas fluorescens. IV. Genetic Constraints Guide Evolutionary Trajectories in a Parallel Adaptive Radiation. *Genetics* 2009; **183**: 1041.
22. Traverse CC, Mayo-Smith LM, Poltak SR, Cooper VS. Tangled bank of experimentally evolved Burkholderia biofilms reflects selection during chronic infections. *Proc Natl Acad Sci U S A* 2013; **110**: E250–E259.
23. Thöming JG, Tomasch J, Preusse M, Koska M, Grahl N, Pohl S, et al. Parallel evolutionary paths to produce more than one Pseudomonas aeruginosa biofilm phenotype. *NPJ Biofilms Microbiomes* 2020; **6**.
24. Leiman SA, Arboleda LC, Spina JS, McLoon AL. SinR is a mutational target for fine-tuning biofilm formation in laboratory-evolved strains of Bacillus subtilis. *BMC Microbiol* 2014; **14**.
25. Dragoš A, Lakshmanan N, Martin M, Horváth B, Maróti G, García CF, et al. Evolution of exploitative interactions during diversification in Bacillus subtilis biofilms. *FEMS Microbiol Ecol* 2018; **94**.

26. Lin Y, Xu X, Maróti G, Strube ML, Kovács ÁT. Adaptation and phenotypic diversification of Bacillus thuringiensis biofilm are accompanied by fuzzy spreader morphotypes. *npj Biofilms Microbiomes 2022 81* 2022; **8**: 1–14.
27. Pomerleau M, Charron-Lamoureux V, Léonard L, Grenier F, Rodrigue S, Beauregard PB. Adaptive laboratory evolution reveals regulators involved in repressing biofilm development as key players in Bacillus subtilis root colonization. *mSystems* 2024; **9**.
28. Ehling-Schulz M, Koehler TM, Lereclus D. The Bacillus cereus Group: Bacillus species with Pathogenic Potential. *Microbiol Spectr* 2019; **7**.
29. Maccario L, Silva AF, Nesme J, Amador CI, Sørensen SJ, Cooper VS, et al. Draft genomes of seven isolates from Danish wastewater facilities belonging to Pseudomonas , Bacillus , Pseudochrobactrum , Brevundimonas , and Pandoraea . *Microbiol Resour Announc* 2023; **12**.
30. Muthukumar A, Raj TS, Prabhukarthikeyan SR, Naveen R, Keerthanab U. Pseudomonas and Bacillus: A biological tool for crop protection. *New Futur Dev Microb Biotechnol Bioeng Sustain Agric Adv Microbe-based Biostimulants* 2022; 145–158.
31. Lyng M, Kovács ÁT. Frenemies of the soil: Bacillus and Pseudomonas interspecies interactions. *Trends Microbiol* 2023; **31**: 845–857.
32. Poltak SR, Cooper VS. Ecological succession in long-term experimentally evolved biofilms produces synergistic communities. *ISME J* 2011; **5**: 369.
33. Herschend J, Koren K, Røder HL, Brejnrod A, Kühl M, Burmølle M. In Vitro Community Synergy between Bacterial Soil Isolates Can Be Facilitated by pH Stabilization of the Environment. *Appl Environ Microbiol* 2018; **84**.
34. Røder HL, Herschend J, Russel J, Andersen MF, Madsen JS, Sørensen SJ, et al. Enhanced bacterial mutualism through an evolved biofilm phenotype. *ISME J* 2018.
35. O'Toole G, Kolter R. Initiation of biofilm formation in Pseudomonas fluorescens WCS365 proceeds via multiple, convergent signalling pathways: a genetic analysis. *Mol Microbiol* 1998; **28**: 449–461.
36. Sprouffske K, Wagner A. Growthcurver: An R package for obtaining interpretable metrics from microbial growth curves. *BMC Bioinformatics* 2016; **17**: 1–4.
37. Toukabri H, Lereclus D, Slamti L. A Sporulation-Independent Way of Life for Bacillus thuringiensis in the Late Stages of an Infection. *MBio* 2023; **14**.

38. Neu T, Kuhlicke U. Fluorescence Lectin Bar-Coding of Glycoconjugates in the Extracellular Matrix of Biofilm and Bioaggregate Forming Microorganisms. *Microorganisms* 2017.

39. Neu TR, Kuhlicke U. Matrix glycoconjugate characterization in multispecies biofilms and bioaggregates from the environment by means of fluorescently-labeled lectins. *Front Microbiol* 2022; **13**.

40. Hartmann R, Jeckel H, Jelli E, Singh PK, Vaidya S, Bayer M, et al. Quantitative image analysis of microbial communities with BiofilmQ. *Nat Microbiol 2021 62* 2021; **6**: 151–156.

41. Liu H, Fang HHP. Extraction of extracellular polymeric substances (EPS) of sludges. *J Biotechnol* 2002; **95**: 249–256.

42. Pan X, Liu J, Zhang D, Chen XI, Li L, Song W, et al. A comparison of five extraction methods for extracellular polymeric substances (EPS) from biofilm by using three-dimensional excitation-emission matrix (3DEEM) fluorescence spectroscopy. *undefined* 2010; **36**: 111–116.

43. Bradford MM. A rapid and sensitive method for the quantitation of microgram quantities of protein utilizing the principle of protein-dye binding. *Anal Biochem* 1976; **72**: 248–254.

44. Herschend J, Damholt ZBV, Marquard AM, Svensson B, Sørensen SJ, Hägglund P, et al. A meta-proteomics approach to study the interspecies interactions affecting microbial biofilm development in a model community. *Sci Rep* 2017.

45. Perez-Riverol Y, Bai J, Bandla C, García-Seisdedos D, Hewapathirana S, Kamatchinathan S, et al. The PRIDE database resources in 2022: a hub for mass spectrometry-based proteomics evidences. *Nucleic Acids Res* 2022; **50**: D543–D552.

46. Deatherage DE, Barrick JE. Identification of mutations in laboratory-evolved microbes from next-generation sequencing data using breseq. *Methods Mol Biol* 2014; **1151**: 165–188.

47. Team. RStudio: Integrated Development for R. *Rstudio, BMC* 2021.

48. Trunk T, Khalil HS, Leo JC. Bacterial autoaggregation. *AIMS Microbiol* 2018; **4**: 140.

49. Amador CI, Canosa I, Govantes F, Santero E. Lack of CbrB in Pseudomonas putida affects not only amino acids metabolism but also different stress responses and biofilm development. *Environ Microbiol* 2010; **12**: 1748–1761.

50. Lopes Da Silva T, Reis A, Kent CA, Roseiro JC, Hewitt CJ. The use of multi-parameter flow cytometry to study the impact of limiting substrate, agitation intensity, and dilution rate on cell aggregation during Bacillus licheniformis CCMI 1034 aerobic continuous culture fermentations. *Biotechnol Bioeng* 2005; **92**: 568–578.
51. Ojima Y, Matano S, Azuma M. Characterization of self-aggregation in Bacillus licheniformis strain RK14. *Ann Microbiol* 2023; **73**: 1–7.
52. Fawcett P, Eichenberger P, Losick R, Youngman P. The transcriptional profile of early to middle sporulation in Bacillus subtilis. *Proc Natl Acad Sci U S A* 2000; **97**: 8063–8068.
53. Molle V, Fujita M, Jensen ST, Eichenberger P, González-Pastor JE, Liu JS, et al. The Spo0A regulon of Bacillus subtilis. *Mol Microbiol* 2003; **50**: 1683–1701.
54. Vollmer W, Blanot D, De Pedro MA. Peptidoglycan structure and architecture. *FEMS Microbiol Rev* 2008; **32**: 149–167.
55. Tännler S, Decasper S, Sauer U. Maintenance metabolism and carbon fluxes in Bacillus species. *Microb Cell Fact* 2008; **7**: 19.
56. Fischer E, Sauer U. Large-scale in vivo flux analysis shows rigidity and suboptimal performance of Bacillus subtilis metabolism. *Nat Genet 2005 376* 2005; **37**: 636–640.
57. Hansen SK, Rainey PB, Haagensen JAJ, Molin S. Evolution of species interactions in a biofilm community. *Nat 2006 4457127* 2007; **445**: 533–536.
58. Cosetta CM, Niccum B, Kamkari N, Dente M, Podniesinski M, Wolfe BE. Bacterial–fungal interactions promote parallel evolution of global transcriptional regulators in a widespread Staphylococcus species. *ISME J 2023 179* 2023; **17**: 1504–1516.
59. Vishnoi M, Narula J, Devi SN, Dao HA, Igoshin OA, Fujita M. Triggering sporulation in Bacillus subtilis with artificial two-component systems reveals the importance of proper Spo0A activation dynamics. *Mol Microbiol* 2013; **90**: 181–194.
60. Huang Y, Flint SH, Palmer JS. Bacillus cereus spores and toxins – The potential role of biofilms. *Food Microbiol* 2020; **90**: 103493.
61. Hamon MA, Lazazzera BA. The sporulation transcription factor Spo0A is required for biofilm development in Bacillus subtilis. *Mol Microbiol* 2001; **42**: 1199–1209.
62. Xu S, Yang N, Zheng S, Yan F, Jiang C, Yu Y, et al. The spo0A-sinI-sinR Regulatory Circuit Plays an Essential Role in Biofilm Formation, Nematicidal Activities, and Plant Protection in Bacillus cereus AR156. *Mol Plant Microbe Interact* 2017; **30**: 603–619.

63. Huang R, Shao J, Xu Z, Chen Y, Liu Y, Wang D, et al. A toxin-mediated policing system in Bacillus optimizes division of labor via penalizing cheater-like nonproducers. *Elife* 2023; **12**: 84743.

64. Sharipova M, Rudakova N, Mardanova A, Evtugyn V, Akosah Y, Danilova I, et al. Biofilm Formation by Mutant Strains of Bacilli under Different Stress Conditions. *Microorganisms* 2023; **11**.

65. Nishikawa M, Kobayashi K. Calcium Prevents Biofilm Dispersion in Bacillus subtilis. *J Bacteriol* 2021; **203**.

66. Rousset L, Alpha-Bazin B, Château A, Armengaud J, Clavel T, Berge O, et al. Groundwater promotes emergence of asporogenic mutants of emetic Bacillus cereus. *Environ Microbiol* 2020; **22**: 5248–5264.

67. Antequera-Gómez ML, Díaz-Martínez L, Guadix JA, Sánchez-Tévar AM, Sopeña-Torres S, Hierrezuelo J, et al. Sporulation is dispensable for the vegetable-associated life cycle of the human pathogen Bacillus cereus. *Microb Biotechnol* 2021; **14**: 1550–1565.

68. Dubois T, Faegri K, Gélis-Jeanvoine S, Perchat S, Lemy C, Buisson C, et al. Correction: Necrotrophism Is a Quorum-Sensing-Regulated Lifestyle in Bacillus thuringiensis. *PLoS Pathog* 2016; **12**.

69. Romero D, Aguilar C, Losick R, Kolter R. Amyloid fibers provide structural integrity to Bacillus subtilis biofilms. *Proc Natl Acad Sci U S A* 2010; **107**: 2230–2234.

70. Branda SS, Chu F, Kearns DB, Losick R, Kolter R. A major protein component of the Bacillus subtilis biofilm matrix. *Mol Microbiol* 2006; **59**: 1229–1238.

71. Lakshmanan V, Kitto SL, Caplan JL, Hsueh Y-H, Kearns DB, Wu Y-S, et al. Microbe-Associated Molecular Patterns-Triggered Root Responses Mediate Beneficial Rhizobacterial Recruitment in Arabidopsis 1[C][W][OA]. *Plant Physiol Ò* 2003; **160**: 1642–1661.

72. Candela T, Fagerlund A, Buisson C, Gilois N, Kolstø AB, Økstad OA, et al. CalY is a major virulence factor and a biofilm matrix protein. *Mol Microbiol* 2019; **111**: 1416–1429.

73. Chen M, Lyu Y, Feng E, Zhu L, Pan C, Wang D, et al. SpoVG Is Necessary for Sporulation in Bacillus anthracis. *Microorganisms* 2020; **8**.

74. Huang Q, Zhang Z, Liu Q, Liu F, Liu Y, Zhang J, et al. SpoVG is an important regulator of sporulation and affects biofilm formation by regulating Spo0A transcription in Bacillus

cereus 0–9. *BMC Microbiol* 2021; **21**: 1–17.

75. Lin Y, Briandet R, Kovács ÁT. Bacillus cereus sensu lato biofilm formation and its ecological importance. *Biofilm* . 2022. , **4**

76. Livingston ET, Mursalin MH, Coburn PS, Astley R, Miller FC, Amayem O, et al. Immune inhibitor a metalloproteases contribute to virulence in Bacillus endophthalmitis. *Infect Immun* 2021; **89**.

77. Harwood CR, Kikuchi Y. The ins and outs of Bacillus proteases: activities, functions and commercial significance. *FEMS Microbiol Rev* 2022; **46**: 1–20.

78. Grandvalet C, Gominet M, Lereclus D. Identification of genes involved in the activation of the Bacillus thuringiensis inhA metalloprotease gene at the onset of sporulation. *Microbiology* 2001; **147**: 1805–1813.

79. Pflughoeft KJ, Sumby P, Koehler TM. Bacillus anthracis sin locus and regulation of secreted proteases. *J Bacteriol* 2011; **193**: 631–639.

80. Hansen LBS, Ren D, Burmølle M, Sørensen SJ. Distinct gene expression profile of Xanthomonas retroflexus engaged in synergistic multispecies biofilm formation. *ISME J* 2017.

81. Ratzke C, Gore J. Modifying and reacting to the environmental pH can drive bacterial interactions. *PLoS Biol* 2018; **16**.

82. Pacheco AR, Segrè D. A multidimensional perspective on microbial interactions. *FEMS Microbiol Lett* 2019; **366**: 125.

83. Aranda-Díaz A, Obadia B, Dodge R, Thomsen T, Hallberg ZF, Güvener ZT, et al. Bacterial interspecies interactions modulate pH-mediated antibiotic tolerance. *Elife* 2020; **9**.

84. Fritts RK, McCully AL, McKinlay JB. Extracellular Metabolism Sets the Table for Microbial Cross-Feeding. *Microbiol Mol Biol Rev* 2021; **85**.

85. Wang M, Yu H, Li X, Shen Z. Single-gene regulated non-spore-forming Bacillus subtilis: Construction, transcriptome responses, and applications for producing enzymes and surfactin. *Metab Eng* 2020; **62**: 235–248.

86. Sonenshein AL. Control of sporulation initiation in Bacillus subtilis. *Curr Opin Microbiol* 2000; **3**: 561–566.

87. Tan IS, Ramamurthi KS. Spore formation in Bacillus subtilis. *Environ Microbiol Rep* 2014; **6**: 212.

88. Grandvalet C, Gominet M, Lereclus D. Identification of genes involved in the activation of the Bacillus thuringiensis inhA metalloprotease gene at the onset of sporulation. *Microbiology* 2001; **147**: 1805–1813.

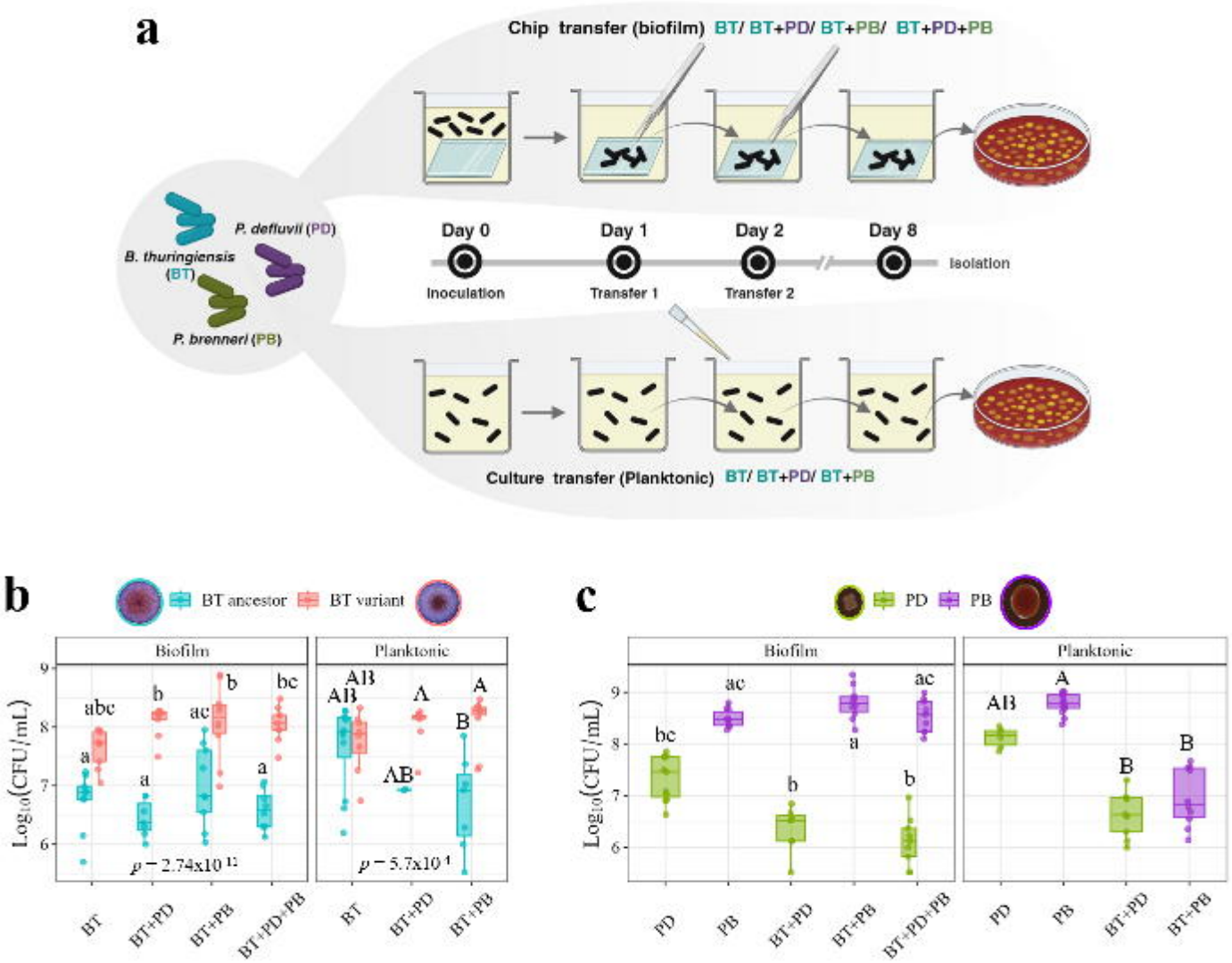
a
Chip transfer (biofilm) BT/ BT+PD/ BT+PB/ BT+PD+PB
P. defluvii (PD)
B. thuringiensis (BT)
P. brenneri (PB)
Day 0
Day 1
Day 2
Day 8
Inoculation
Transfer 1
Transfer 2
Isolation
Culture transfer (Planktonic) BT/ BT+PD/ BT+PB
b
BT ancestor
BT variant
Biofilm
Planktonic
Log10(CFU/mL)
p = 2.74x10-12
p = 5.7x10-4
BT
BT+PD
BT+PB
BT+PD+PB
c
PD
PB
Biofilm
Planktonic
Log10(CFU/mL)
PD
PB
BT+PD
BT+PB
BT+PD+PB

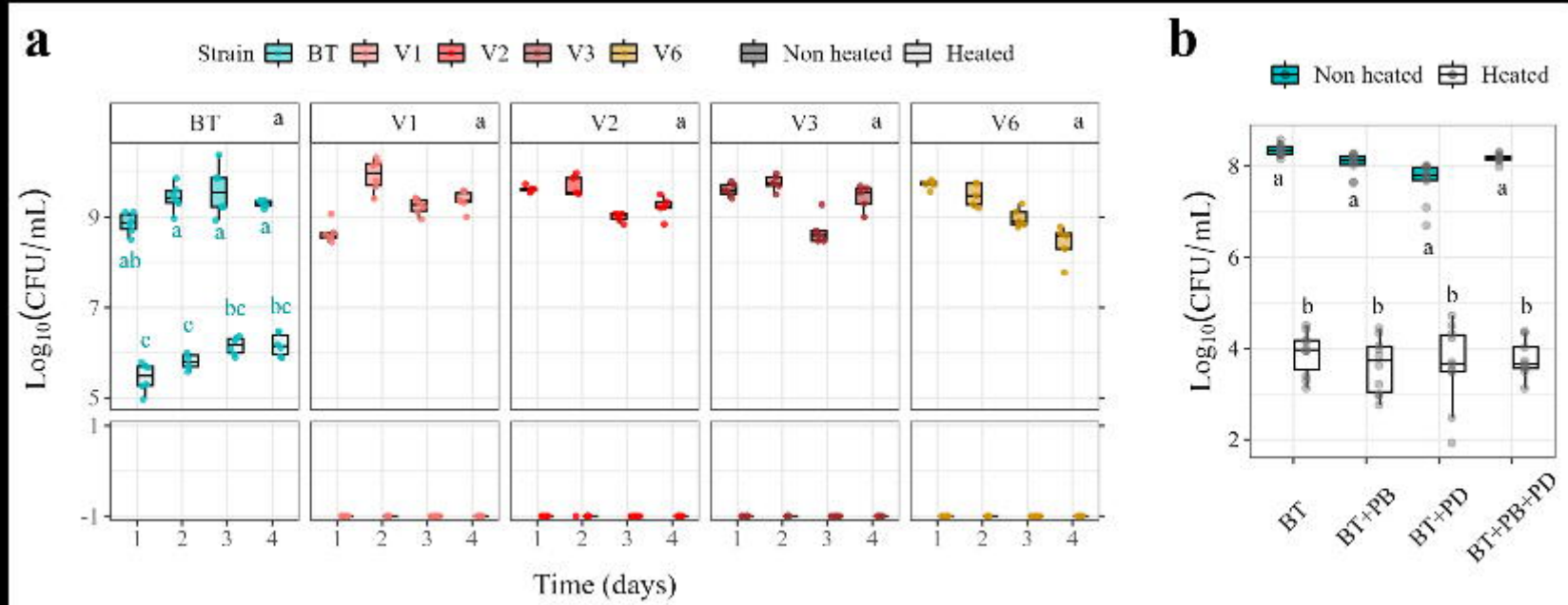
a
Strain BT V1 V2 V3 V6
Non heated Heated
BT
V1
V2
V3
V6
Log10(CFU/mL)
Time (days)
b
Non heated Heated
Log10(CFU/mL)
BT
BT+PB
BT+PD
BT+PB+PD

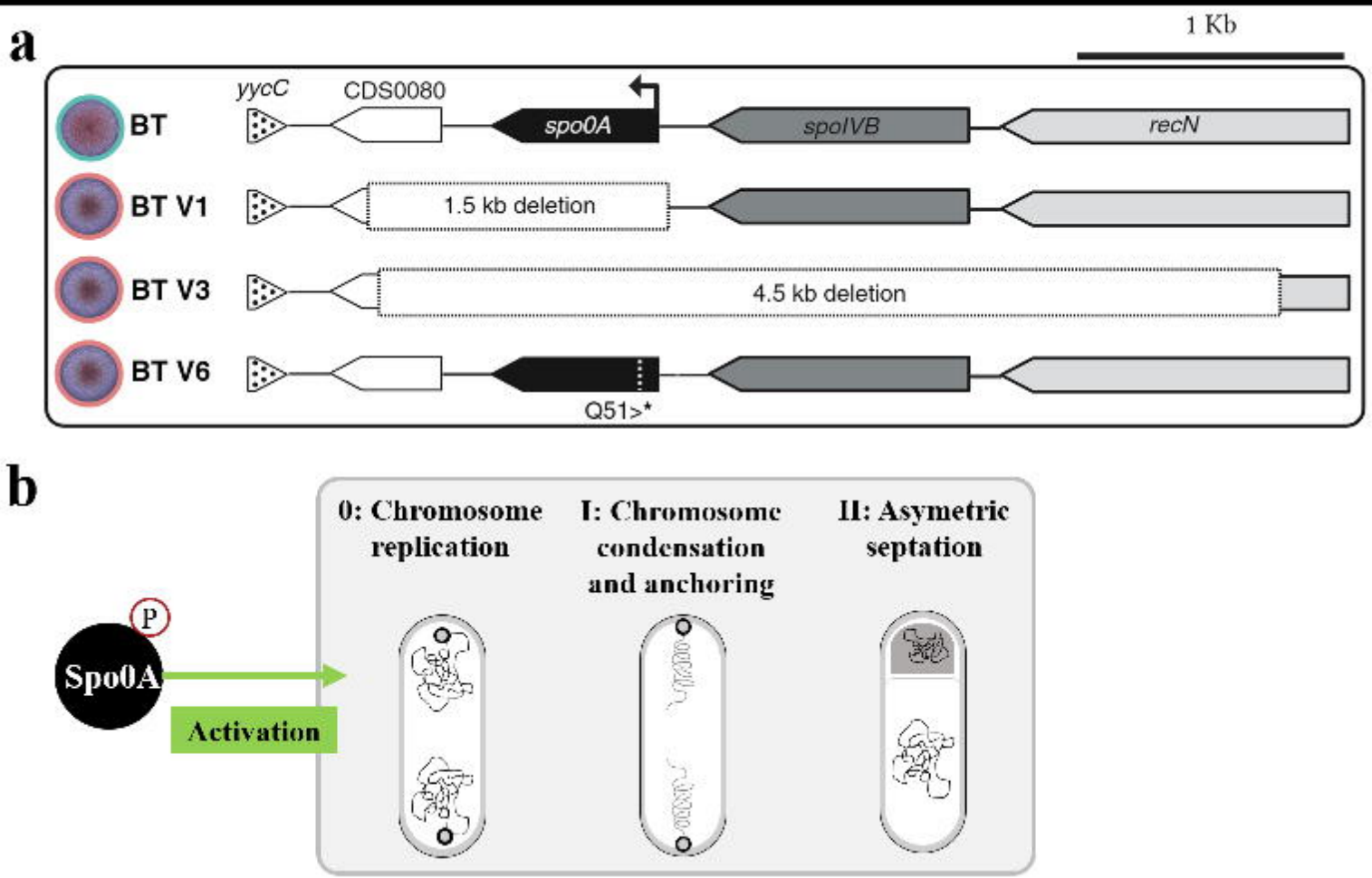
a
1 Kb
yycC
CDS0080
spo0A
spoIVB
recN
BT
BT V1
1.5 kb deletion
BT V3
4.5 kb deletion
BT V6
Q51>*
b
0: Chromosome replication
I: Chromosome condensation and anchoring
II: Asymetric septation
P
Spo0A
Activation

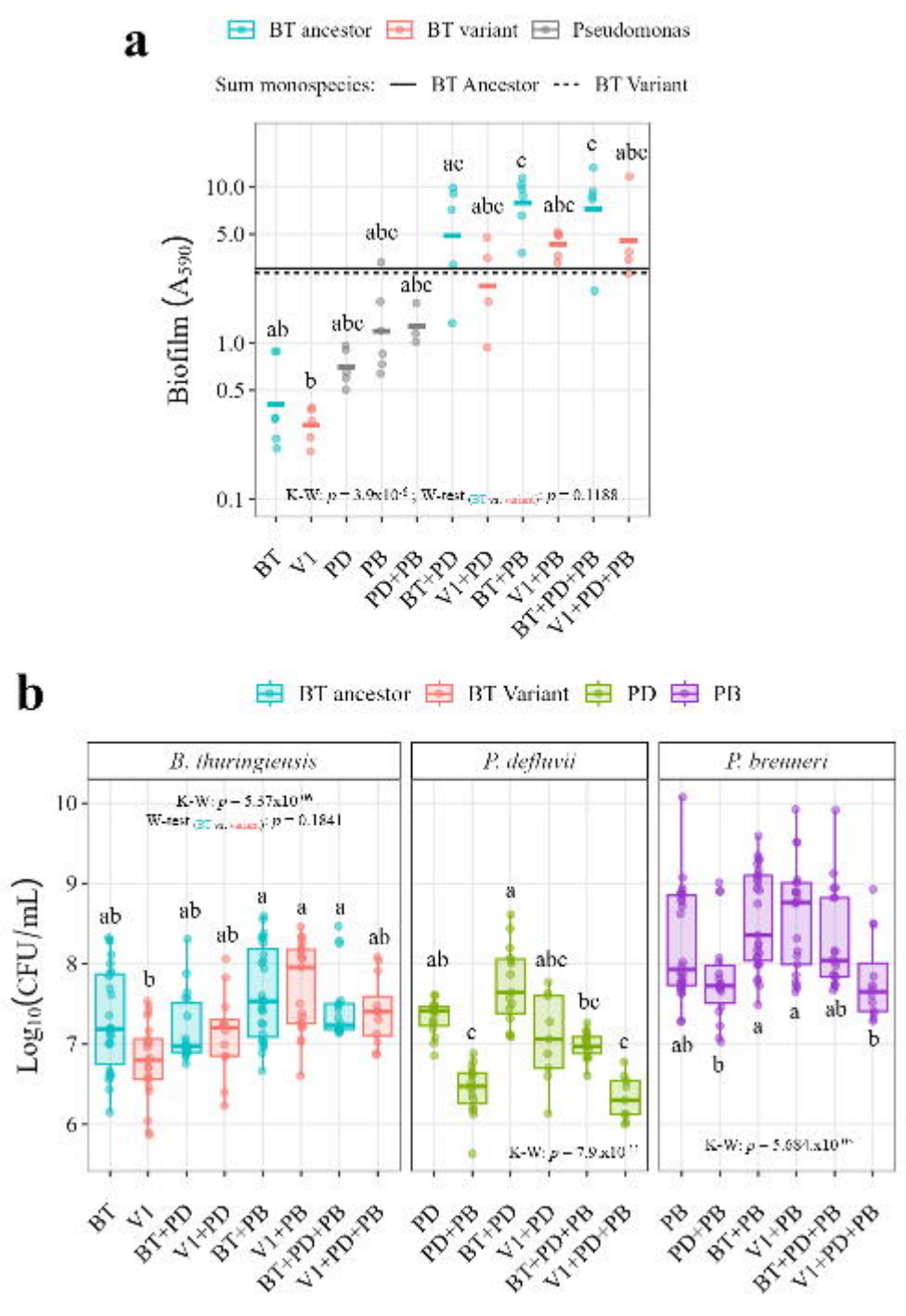
a
BT ancestor
BT variant
Pseudomonas
Sum monospecies:
BT Ancestor
BT Variant
Biofilm (A_{590})
10.0
5.0
1.0
0.5
0.1
ab
b
abc
abc
abc
ac
abc
c
abc
c
abc
K-W: $p = 3.9x10^{-5}$; W-test $_{(BT\ vs.\ variant)}$: $p = 0.1188$
BT
V1
PD
PB
PD+PB
BT+PD
V1+PD
BT+PB
V1+PB
BT+PD+PB
V1+PD+PB
b
BT ancestor
BT Variant
PD
PB
B. thuringiensis
P. defluvii
P. brenneri
Log_{10}(CFU/mL)
10
9
8
7
6
K-W: $p = 5.57x10^{-16}$
W-test $_{(BT\ vs.\ variant)}$: $p = 0.1841$
ab
b
ab
ab
a
a
a
ab
ab
c
a
abc
bc
c
ab
b
a
a
ab
b
K-W: $p = 7.9x10^{-11}$
K-W: $p = 5.68x10^{-16}$
BT
V1
BT+PD
V1+PD
BT+PB
V1+PB
BT+PD+PB
V1+PD+PB
PD
PD+PB
BT+PD
V1+PD
BT+PD+PB
V1+PD+PB
PB
PD+PB
BT+PB
V1+PB
BT+PD+PB
V1+PD+PB

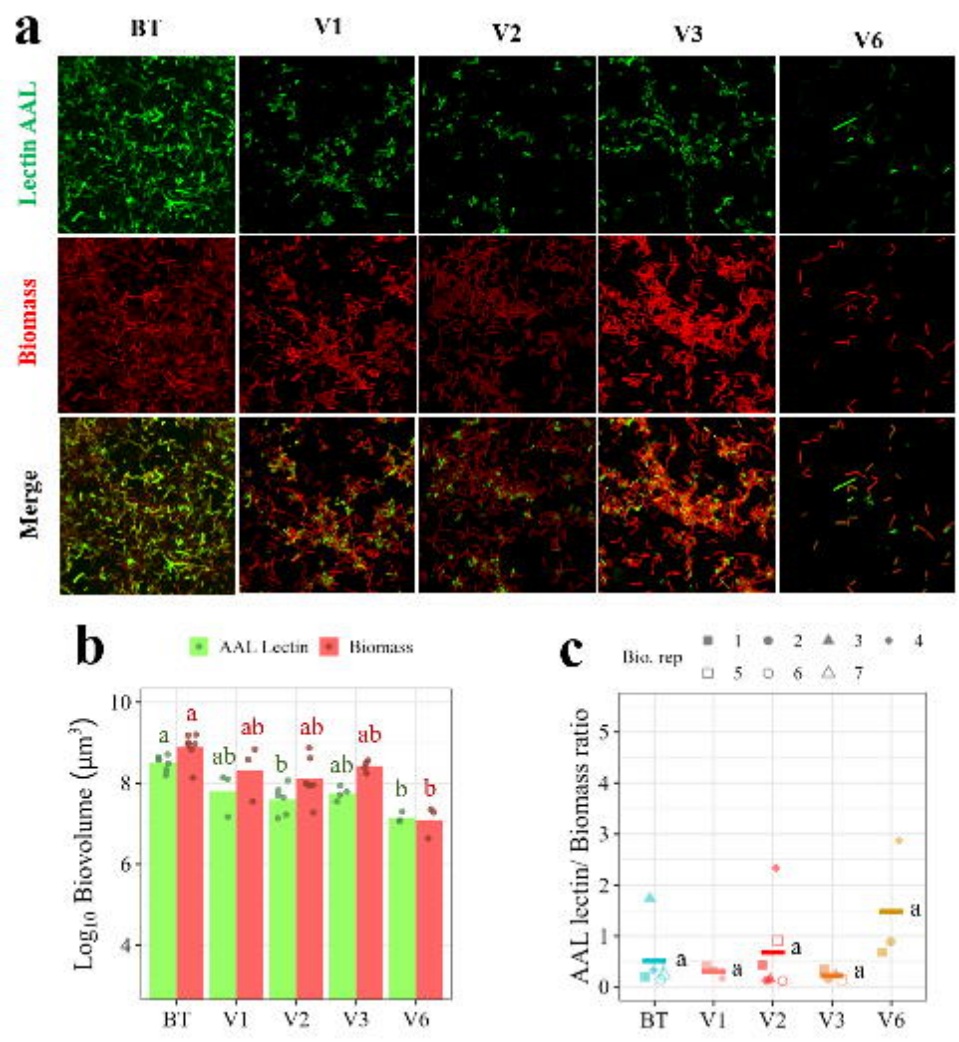
a
BT
V1
V2
V3
V6
Lectin AAL
Biomass
Merge
b
AAL Lectin
Biomass
Log10 Biovolume (μm3)
10
8
6
4
a
a
ab
ab
b
ab
ab
ab
b
b
BT
V1
V2
V3
V6
c
Bio. rep
1
2
3
4
5
6
7
AAL lectin/ Biomass ratio
5
4
3
2
1
0
a
a
a
a
a
BT
V1
V2
V3
V6

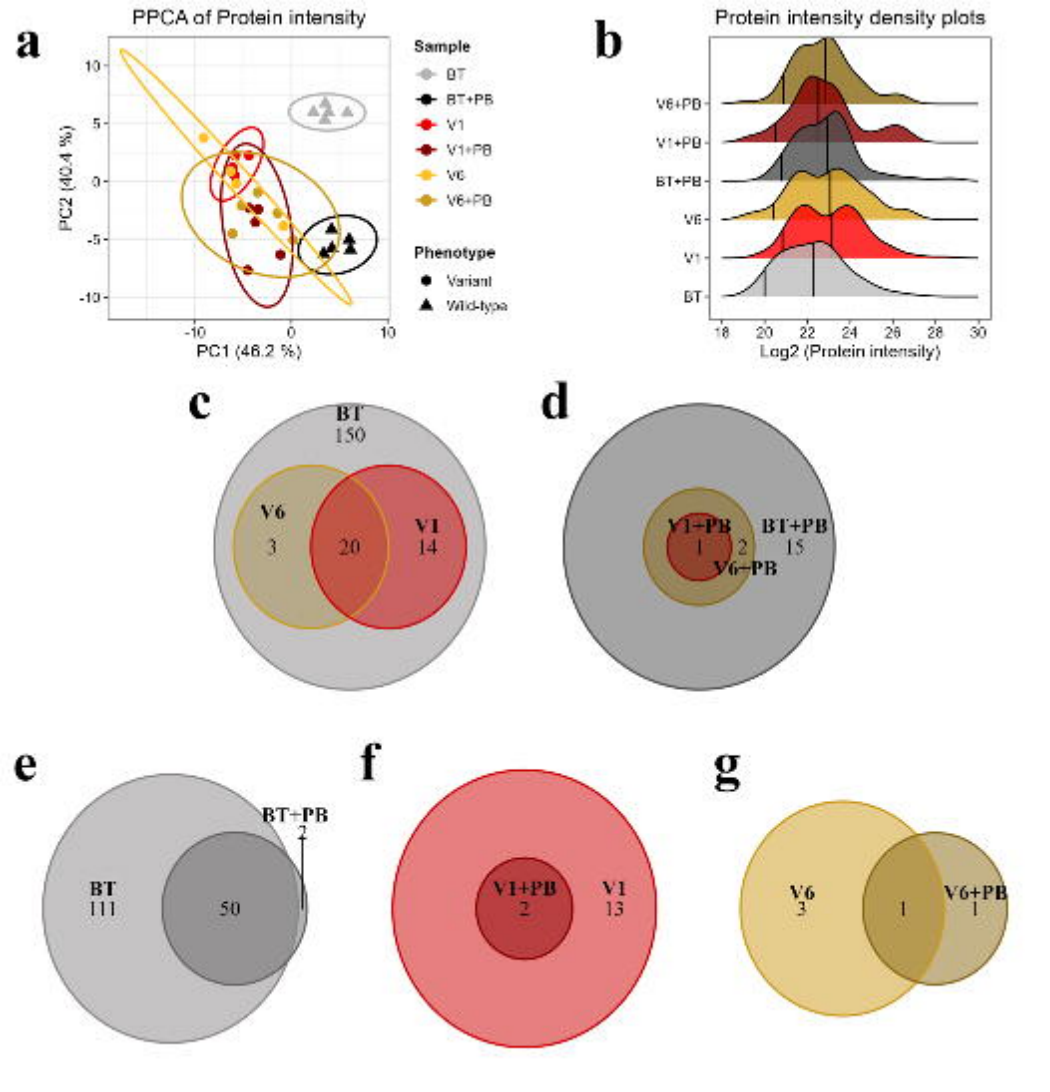
a
PPCA of Protein intensity
PC2 (40.4 %)
PC1 (46.2 %)
Sample
BT
BT+PB
V1
V1+PB
V6
V6+PB
Phenotype
Variant
Wild-type
b
Protein intensity density plots
V6+PB
V1+PB
BT+PB
V6
V1
BT
Log2 (Protein intensity)
c
BT
150
V6
3
20
V1
14
d
V1+PB
1
2
BT+PB
15
V6+PB
e
BT+PB
2
BT
111
50
f
V1+PB
2
V1
13
g
V6
3
1
V6+PB
1

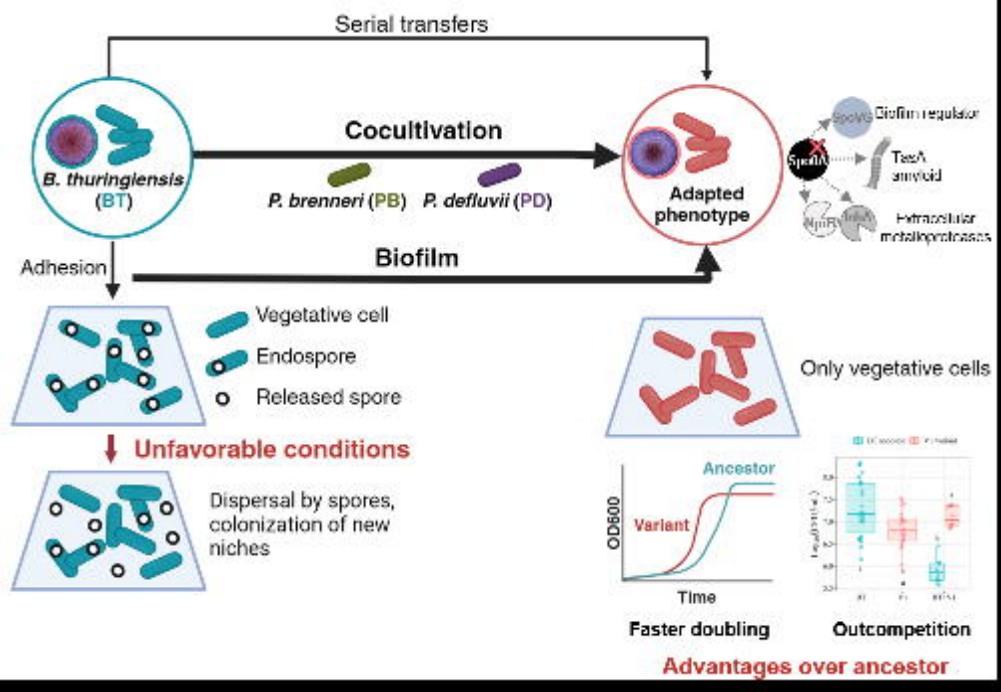

Serial transfers
Cocultivation
B. thuringiensis (BT)
P. brenneri (PB)
P. defluvii (PD)
Adapted phenotype
Biofilm regulator
TasA amyloid
Extracellular metalloproteases
Adhesion
Biofilm
Vegetative cell
Endospore
Released spore
Unfavorable conditions
Dispersal by spores, colonization of new niches
Only vegetative cells
Ancestor
Variant
OD600
Time
Faster doubling
Outcompetition
Advantages over ancestor

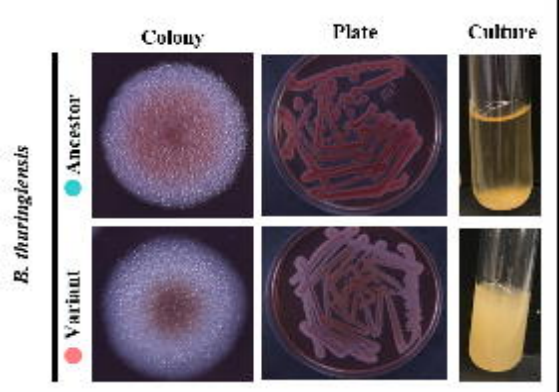
Colony
Plate
Culture
B. thuringiensis
Ancestor
Variant

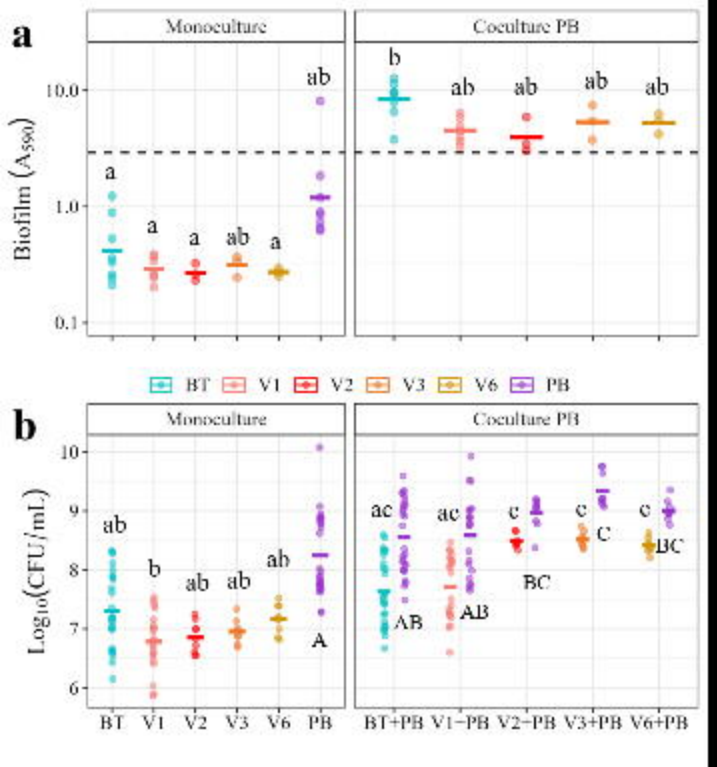
a
Monoculture
Coculture PB
Biofilm (A_{590})
10.0
1.0
0.1
a
a
a
ab
a
ab
b
ab
ab
ab
ab
BT
V1
V2
V3
V6
PB
b
Monoculture
Coculture PB
Log_{10}(CFU/mL)
10
9
8
7
6
ab
b
ab
ab
ab
A
ac
AB
ac
AB
c
BC
c
C
c
BC
BT
V1
V2
V3
V6
PB
BT+PB
V1+PB
V2+PB
V3+PB
V6+PB

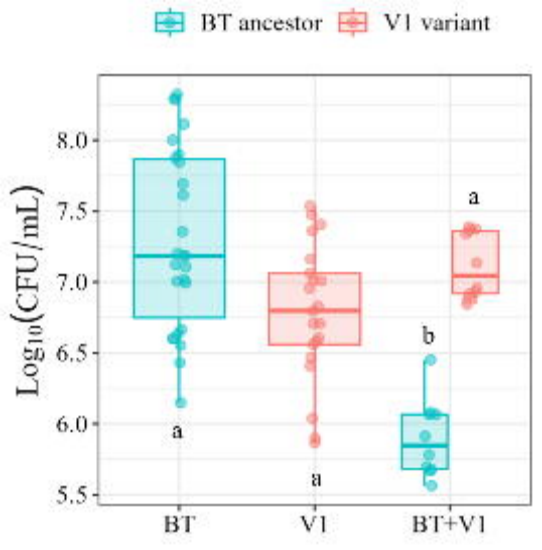
BT ancestor
V1 variant
Log10(CFU/mL)
8.0
7.5
7.0
6.5
6.0
5.5
a
a
b
a
BT
V1
BT+V1

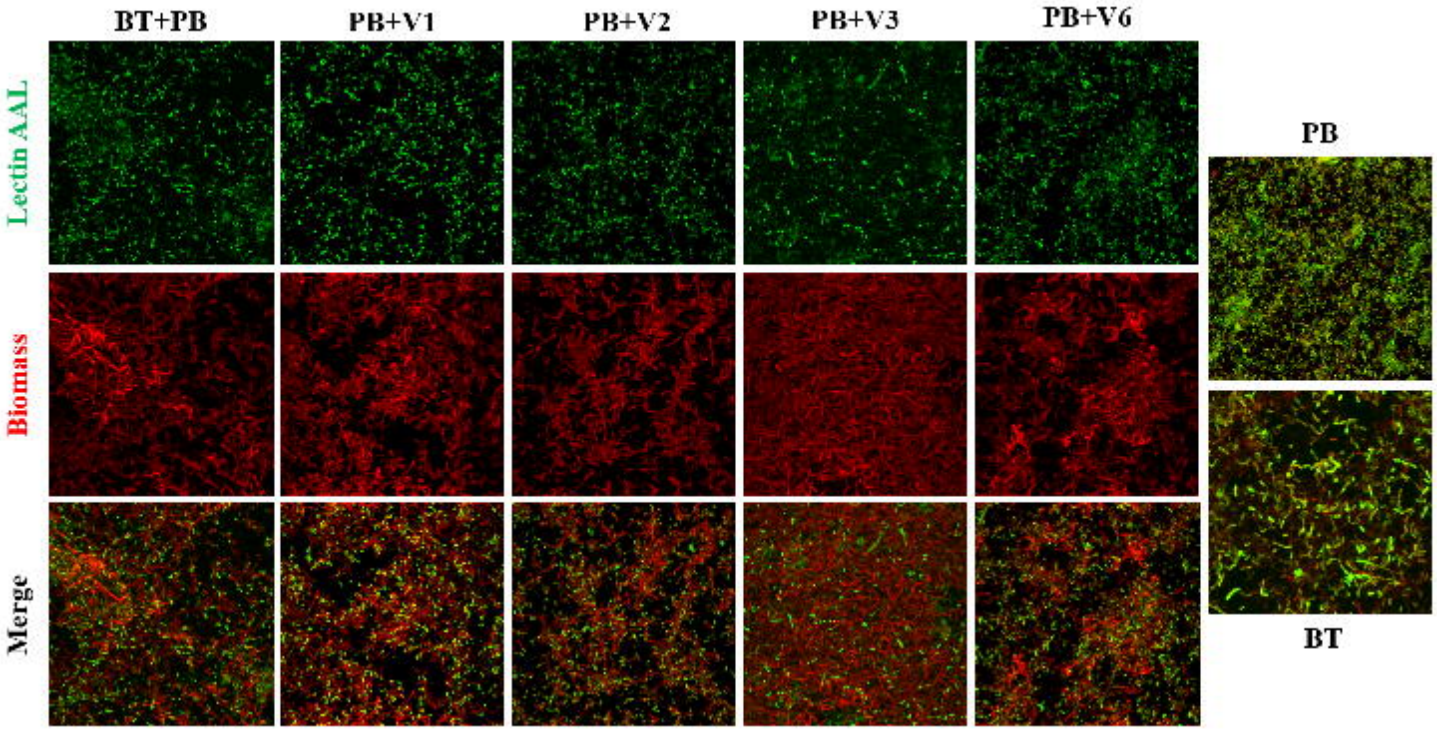
BT+PB
PB+V1
PB+V2
PB+V3
PB+V6
Lectin AAL
Biomass
Merge
PB
BT

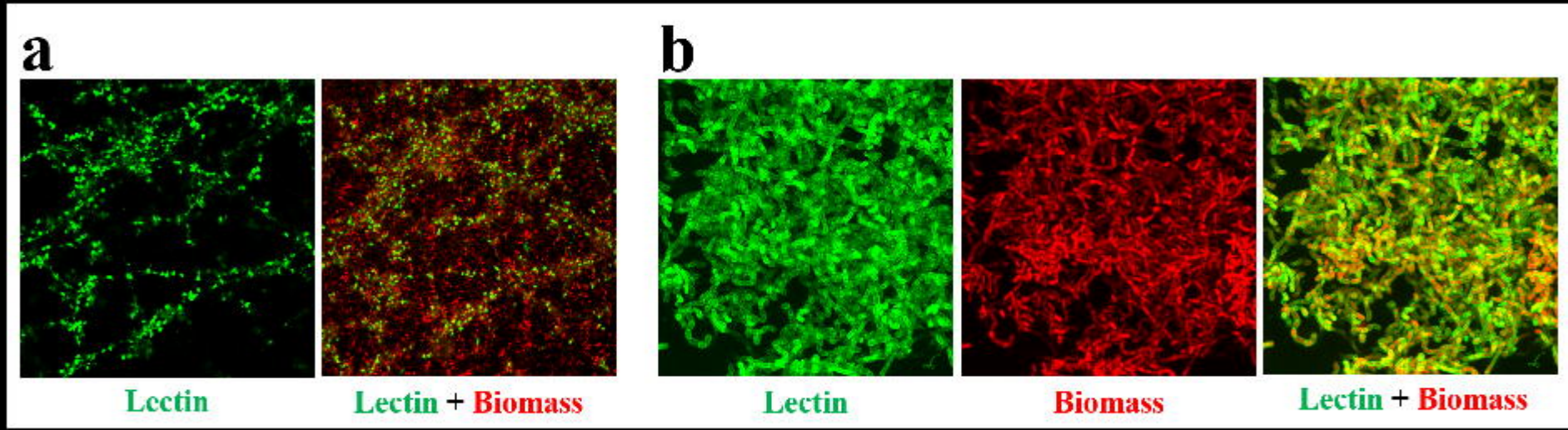
a
b
Lectin
Lectin + Biomass
Lectin
Biomass
Lectin + Biomass

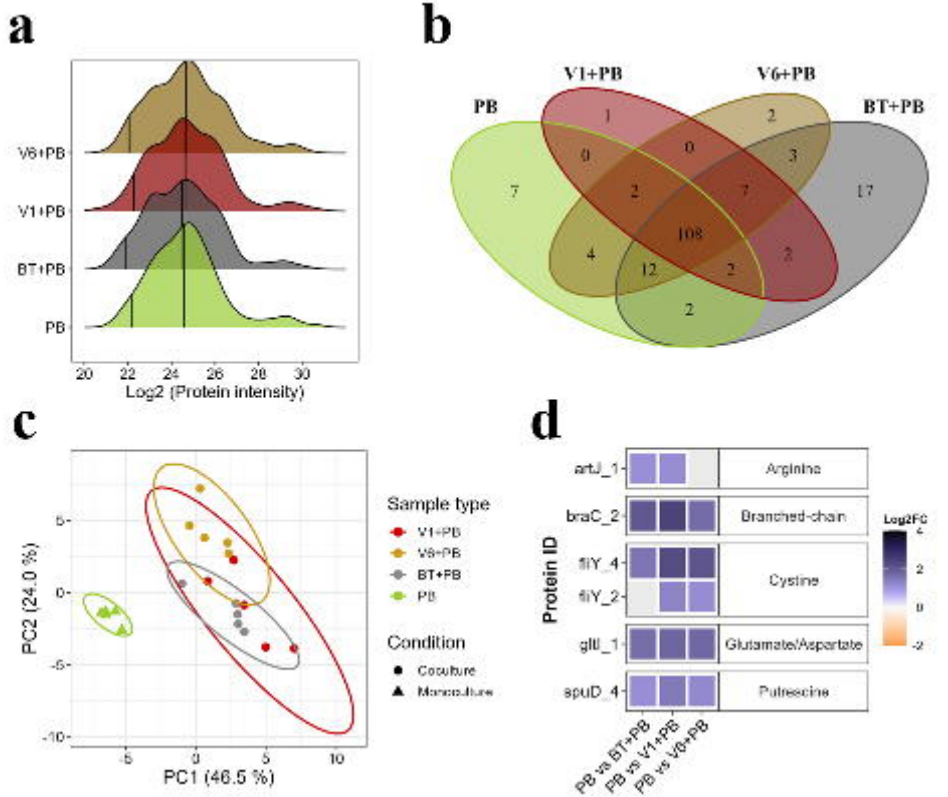
a
V6+PB
V1+PB
BT+PB
PB
20
22
24
26
28
30
Log2 (Protein intensity)
b
PB
V1+PB
V6+PB
BT+PB
7
1
0
0
2
3
17
2
7
108
4
12
2
2
2
c
PC2 (24.0 %)
PC1 (46.5 %)
Sample type
V1+PB
V6+PB
BT+PB
PB
Condition
Coculture
Monoculture
d
Protein ID
artJ_1
braC_2
fliY_4
fliY_2
gltI_1
spuD_4
Arginine
Branched-chain
Cystine
Glutamate/Aspartate
Putrescine
Log2FC
PB vs BT+PB
PB vs V1+PB
PB vs V6+PB

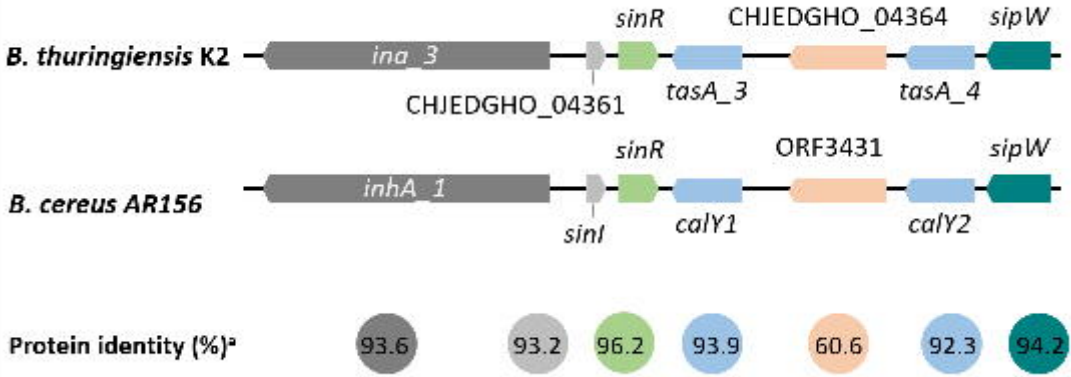
B. thuringiensis K2
ina_3
CHJEDGHO_04361
sinR
tasA_3
CHJEDGHO_04364
tasA_4
sipW
B. cereus AR156
inhA_1
sinI
sinR
calY1
ORF3431
calY2
sipW
Protein identity (%)[a]
93.6
93.2
96.2
93.9
60.6
92.3
94.2